scientific reports

Check for updates

OPEN

Investigation of smoothed particle hydrodynamics (SPH) method for modeling of two-phase flow through porous medium: application for drainage and imbibition processes

Masoud Mohammadi[1], Masoud Shafiei[1], Taha Zarin[1], Yousef Kazemzadeh[2,3]✉, Rafat Parsaei[1]✉ & Masoud Riazi[2,4]✉

The drainage and imbibition processes are critical mechanisms in petroleum engineering. These processes in a porous medium are controlled by surface forces and pressure gradients. The study of these processes in the pore scale by common simulators always has limitations in multiphase flow modeling. Also, obtaining relative permeability curves through laboratory analysis requires expensive equipment. Additionally, these laboratory experiments are quite expensive and may introduce significant uncertainties. For this purpose, this study investigated the creation of relative permeability curves and their effect on oil production. Initially, single-phase fluid and two-phase droplet flow within a fracture with both soft and rough surfaces were utilized to validate the formulation of the Smoothed Particle Hydrodynamics (SPH) method. Then, by using three randomly constructed porous medium models, the imbibition and drainage processes have been studied. Finally, sensitivity study has been carried out on critical parameters related to fluid flow dynamics in the porous environment, including pressure changes, wettability, and heterogeneity in drainage and imbibition processes. The simulation results were consistent with current theories; therefore, it is reasonable to consider SPH to characterize the fluid flow dynamic during the drainage and imbibition processes. According to sensitivity studies, pressure gradient (residual saturation of displaced fluid is about 5.65% and 8.44%) and heterogeneity (the residual saturation of the displaced fluid was 4.04% and 2.98%) have the largest impact on flow modeling in both drainage and imbibition processes and wettability (the residual saturation became 36.62% and 5.12%) has significant effect on the drainage process through porous medium. In general, fluid flow dynamic studies can be performed using the SPH method to model fluid flow in simple and complex porous medium under various flow conditions. The SPH method can also be used as an applicable tool to investigate the hydrocarbon fluids flow within larger geometries in the future.

Keywords Smoothed particle hydrodynamics, Porous medium, Non-mixing multiphase flow, Drainage, Imbibition

Forced drainage and spontaneous imbibition tests are among the most significant rock and fluid laboratory tests in petroleum engineering; However, these tests are expensive and time-consuming, making modeling inevitable. An increase in the saturation of the non-wetting phase results from drainage that is entirely reciprocal, which often involves increased use of energy. On the other hand, the imbibition process, as spontaneous or forced,

[1]Department of Petroleum Engineering, School of Chemical and Petroleum Engineering, Shiraz University, Shiraz, Iran. [2]Enhanced Oil Recovery (EOR) Research Centre, IOR-EOR Research Institute, Shiraz University, Shiraz, Iran. [3]Department of Petroleum Engineering, Faculty of Petroleum, Gas, and Petrochemical Engineering, Persian Gulf University, Bushehr, Iran. [4]School of Mining and Geosciences, Nazarbayev University, 010000 Astana, Kazakhstan. ✉email: yusefkazemzade@yahoo.com; rparsaei@shirazu.ac.ir; masoud.riazi@nu.edu.kz

is a process in which the saturation of the wetting phase is enhanced through the displacement of the non-wetting phase within porous medium. Multi-phase and multi-component fluids flow through heterogeneous porous medium can be governed by a series of nonlinear equations (momentum conservations) which come with some limitations. The role of modeling for fluid flow through porous medium is important because of the limitations of laboratory and experimental studies, with their specific limitations, the complex geometry, and multi-interfaces[1].

SPH was originally introduced by Lucy[2], and then Monaghan[3] to model astronomical problems. This method has lately been employed for the numerical modeling of multiphase flows through porous medium[4]. The key benefits of SPH, which Monaghan first suggested in 1992[5] to represent fluid dynamics, include: (a) SPH is a fully Lagrangian method, and the momentum conservation equation does not involve the nonlinear convection term; therefore, as a result of the convection term being discretized, there is no numerical dispersion. (b) It is not necessary to explicitly track and record the interface between different phases (no need for a tracking algorithm)[6]. (c) The dynamic contact line does not require a phenomenological model. (d) SPH discretization scheme simplifies parallel treatment by reducing the Navier–Stokes equations to a system of ordinary differential equations (ODE). SPH approach also has some disadvantages: (a) SPH is designed for compressible flows. Therefore, extra techniques are required for incompressible flows to boost algorithm stability. (b) In general, SPH technique costs more to compute than grid-based methods since it involves more nearby particles in the discretization of spatial derivatives than grid-based methods due to the smaller number of grid points[1].

Traditional and common simulation methods have problems such as convergence, high CPU time, and high complexity. In recent years, particle-based methods such as SPH have gained much attention due to higher order convergence, lower CPU time, less complexity, and higher accuracy in the results. SPH has been recently developed to model problems at any scale for the flow of fluids through porous medium at low Reynolds numbers conditions[7–9]. Zhu et al. introduced SPH as a technique with the potential to predict the mesoscopic and microscopic characteristics of pores of porous medium. Tartakovsky and Meakin[10] used SPH to model the unsaturated flow within fractures with complex geometry. Then, they developed SPH to model immiscible and miscible fluid flow through porous medium. The effects of pore scale heterogeneity and anisotropy have also been investigated and discussed using SPH[11]. According to Holmes et al.[12], SPH can conduct numerical tests to investigate the impact of surfactant and water injection on oil recovery as well as the potential for developing new methods to improve oil recovery. Holmes et al. also[13] investigated the use of SPH to characterize fluid flow with low Reynolds numbers through ideal and real porous medium generated from 3D X-ray microtomography images. The application of SPH to characterize rock properties is demonstrated by calculating friction and permeability coefficients. The study of Kunz et al.[14] showed a high consistency of SPH results with the findings of experimental tests. The importance of using mathematical models, like SPH was emphasized by Sigalotti et al.[15]. Additionally, the fluid–fluid-solid contact line dynamics and wetting behavior are studied using SPH[16]. Tartakovsky and Panchenko[16] comprehensively outlined the fundamentals of SPH for modeling multiphase fluid flows within the reservoir, along with its most recent advancements and applications. Also, Su et al.[1] and Golparvar et al.[17] investigated the latest developments in fluid flow modeling through porous medium in the pore scale. They have introduced SPH as one of the alternatives for modeling fluid flow in the pore scale together with other numerical methods such as the pore network and lattice-Boltzmann model. Also, they showed the ability of SPH to characterize reservoir fluid flow through porous medium. Lately, Liu et al.[18] modeled the imbibition phenomena within a porous medium for liquid and gas flow using SPH method. They used contact angle analysis to verify, but they did not evaluate the drainage process alongside the complete analysis of both processes. SPH has also been applied in many other fields. Recently, Bingbai et al.[19] employed SPH for modeling electrical conductivity in complex porous systems. They conducted a comparison of SPH results with experiments, and the findings show a good agreement with experiments. Mohammadi and Riazi[20] also used SPH to characterize fluid flow through porous medium and obtained applicable relationships for the permeability, and hydraulic tortuosity. Considering that it is a straightforward method and does not require much initial information, it is suitable for complex geometries and has an easier initialization.

So far, various modeling methods have been developed for the characterization of the multiphase fluid flow through porous medium. Investigating parameters such as relative permeability and developing relative permeability curves is a critical aspect ofstudying multiphase flow. In addition, these methods require complex and expensive equipment, which can limit their application. In this research, the development of relative permeability curves and the study of their effect on oil production have been conducted using the SPH method. To the best of our knowledge, no studies have applied the SPH method to model and characterize the reservoir fluid flow through the reservoir rock for the drainage and imbibition processes as the main flowing mechanisms. In this study, it has been attempted to demonstrate the potential and simplicity of using the SPH method to solve the complex problems of the petroleum industry. The modeling was done using a collection of formulations applied in the literature. At first, SPH formulation was validated in regular models with analytical theories. Then, the SPH method was employed to characterize the drainage and imbibition processes in the complex and irregular porous medium. Some two-phase hydrocarbon fluid flow modeling of oil and water in three types of porous medium with randomly generated structures were investigated. Finally, sensitivity analysis was performed on key parameters related to the dynamics of fluid flow through porous medium during both drainage and imbibition processes.

Smoothed particle hydrodynamics

Formulation of smoothed particle hydrodynamics

According to the study by Monaghan[5] and Liu and Liu[21], the main idea behind SPH is the introduction of kernel interpolants for the field quantities so that the fluid dynamics is represented by a series of particle evolution equations. The first is the interpolation of the field quantities A(r) at a point as follows,

$$A(r) = \int A(r')W(r - r')dr' \tag{1}$$

where W is a weighting or kernel function, and the integration is performed across the entire modeling domain. The weighting function is constrained with the parameter *h* called the smoothing length. In general, the kernel function must resemble a Gaussian satisfying criterion, being normalized, and sufficiently smooth in addition to being an even (symmetric) function. The second approximation of SPH model is the discretization of the main domain which is done by dividing the porous medium into a set of particles. The field quantities are carried by each particle. In this way, the integral interpolant in Eq. (1) becomes then the summation of the interpolant as follows,

$$A_i = \sum_{j=1}^{N} \frac{m_j}{\rho_j} A_j \cdot W\left(\left|\overrightarrow{r}_i - \overrightarrow{r}_j\right|.h\right) = \sum_{j=1}^{N} \frac{m_j}{\rho_j} A_j \cdot W(R.h) = \sum_{j=1}^{N} \frac{m_j}{\rho_j} A_j \cdot W_{ij}^{h} \tag{2}$$

where N is the total number of particles, m_j and ρ_j are the masses and densities of particle j at position r_j, respectively, and R is the relative distance between the pair of neighboring particles i and j. To keep the continuous and discrete forms of the field expression consistent, the fraction m_j/ρ_j accounts for the approximate volume of space occupied by each particle. Correspondingly, the gradient of field quantity A is given by,

$$\overrightarrow{\nabla} A_i = \sum_{j=1}^{N} \frac{m_j}{\rho_j} A_j \cdot \overrightarrow{\nabla}_i W\left(\left|\overrightarrow{r}_i - \overrightarrow{r}_j\right|.h\right) = \sum_{j=1}^{N} \frac{m_j}{\rho_j} A_j \cdot \overrightarrow{\nabla}_i W_{ij}^{h} \tag{3}$$

Tartakovsky and Meakin[10], Solenthaler and Pajarola[22] presented the particle number density, n, to replace, m/ρ and proved that this technique may eliminate the artificial surface tension induced by the high-density ratio at the fluid–fluid interface.

$$n_i = \frac{\rho_i}{m_i} \text{ and } A_i = \sum_{j=1}^{N} \frac{A_j}{n_j} W_{ij}^{h} \text{ and } \vec{\nabla} A_i = \sum_{j=1}^{N} \frac{A_j}{n_j} \vec{\nabla}_i W_{ij}^{h} \tag{4}$$

According to the differential quotient or product expansion form, the gradient term can be rewritten by introducing the density by the differential operator with the following formula. Due to the pairwise anti-symmetric formulation, the gradient and Laplacian terms are stated as a pair of particles and are conservative,

$$\vec{\nabla} A_i = \sum_{j=1}^{N} \left(\frac{A_j}{n_j^2} + \frac{A_i}{n_i^2}\right) \vec{\nabla}_i W_{ij}^{h} \text{ and } \vec{\nabla}^2 A_i = \sum_{j=1}^{N} \frac{(A_i - A_j)}{n_i n_j \left|\vec{r}_i - \vec{r}_j\right|^2} \left(\vec{r}_i - \vec{r}_j\right) \cdot \vec{\nabla}_i W_{ij}^{h} \tag{5}$$

For more accuracy in term of Laplacian, we used the hybrid method. The continuity and momentum equations are the base of the all of governing equations for fluid flows as follows,

$$\frac{d\rho}{dt} = -\rho\left(\vec{\nabla} \cdot \vec{u}\right) \text{ and } \frac{d\vec{u}}{dt} = -\frac{1}{\rho}\vec{\nabla} p + \frac{1}{\rho}\nabla \cdot \left[\left(\mu\left(\nabla \vec{u} + \nabla \vec{u}^{\tau}\right) - \frac{2}{d}\mu\left(\nabla \cdot \vec{u}\right) I\right)\right] + m\vec{g} + \vec{f}^{Ext} \tag{6}$$

where superscript τ denotes transposition, u is the velocity, t is the time, ρ is the density, p is the pressure, μ is the kinematic viscosity, d is the dimension, I is the identity tensor, g is the gravitational acceleration, and f is the sum of external forces. In case of incompressible fluid flow the continuity and momentum equations become Navier–Stokes as follows,

$$\frac{d\rho}{dt} = 0 \text{ and } \frac{d\vec{u}}{dt} = -\frac{1}{\rho}\vec{\nabla} p + \frac{\mu}{\rho}\nabla^2 \vec{u} + m\vec{g} + \vec{f}^{Ext} \tag{7}$$

Using Eqs. (2) to (5), the Navier–Stokes Eqs. (7) can be discretized as follow, (The Eulerian fundamental continuity and motion equations have been transformed into the Lagrangian form and smoothed particle hydrodynamic model explain by Tartakovsky and Meakin[11].)

$$\rho_i = m_i \sum_{j=1}^{N} W_{ij}^{h} = m_i \cdot n_i \tag{8}$$

$$m_i \frac{d\overrightarrow{u}_i}{dt} = -\sum_{j=1}^{N} \left(\frac{p_j}{n_j^2} + \frac{p_i}{n_i^2}\right) \cdot \overrightarrow{\nabla}_i W_{ij}^{h} + 2\mu \sum_{j=1}^{N} \frac{\left(\overrightarrow{u}_i - \overrightarrow{u}_j\right)}{n_i n_j \left|\overrightarrow{r}_i - \overrightarrow{r}_j\right|^2} \left(\overrightarrow{r}_i - \overrightarrow{r}_j\right) \cdot \overrightarrow{\nabla}_i W_{ij}^{h} + m_i \overrightarrow{g} + \overrightarrow{f}_i^{Ext} \tag{9}$$

Similar to the summation density method used in traditional SPH, Eq. (8) represents continuity conservation and conserves mass exactly. The acting force on all particles at each time step can be calculated by Eq. (9). A linear Equation of State (EOS) proposed by Tartakovsky and Meakin[11] is used in this study to determine pressure for an incompressible fluid. In this study, we used the reduced parameters that were obtained in comparison to

an optional reference condition. The reference value for the length is equal to the smoothing length, 1 s is chosen as the reference value for time, and the basic properties of mass and viscosity are also chosen to be equal to their values. Based on the above explanation, it is possible to understand the basics of using reduced units and the relationship between reduced units and actual physical values. The advantage of using reduced units is that it allows generalization of results and does not limit the obtained results to specific values. In other words, the obtained results can be used in a general way. Also, the fourth-order kernel function with constant smoothing length was employed[23]:

$$W(R,h)=\frac{63}{478\pi h^2}\begin{cases}(3-R)^5-6(2-R)^5+15(1-R)^5 & 0\le R<1\\ (3-R)^5-6(2-R)^5 & 1\le R<2\\ (3-R)^5 & 2\le R<3\\ 0 & R\ge 3\end{cases}\quad \text{and } R=\frac{|\vec{r}_i-\vec{r}_j|}{h} \tag{10}$$

We employ Pairwise Force SPH (PF-SPH) formulation introduced by Tartakovsky and Panchenko[16] to model interfacial tension and wettability forces due to the Young–Laplace and Young boundary conditions. The interaction force between a pair of particles i and j ($f_i^{Ext}=F_{ij}^{int}$) in the PF-SPH formulation is given by,

$$\begin{aligned}\vec{f}_i^{Ext}&=\sum_j^N\left[S_{ij}\left(8e^{-\left(|\vec{r}_i-\vec{r}_j|^2/2\varepsilon^2\right)}-e^{-\left(|\vec{r}_i-\vec{r}_j|^2/2\varepsilon_0^2\right)}\right)(\vec{r}_i-\vec{r}_j)\right]\\ &\text{and } \frac{\varepsilon}{\varepsilon_0}=2 \text{ and } \varepsilon=\frac{h}{3.5} \text{ and } |\vec{r}_i-\vec{r}_j|\le h\end{aligned} \tag{11}$$

where S_{ij} is the strength of the interaction force. The sum of all pair forces gives the total force resulting from inter-particle interactions occurring on particle i. Parameterization of the PF-SPH formulation (for surface tension and static contact angle), and estimating the magnitude of the pair forces at fluid–fluid and fluid–fluid-solid interfaces are also taken from the method introduced by Tartakovsky and Panchenko[16] with the assumptions $n_\alpha=n_\beta=n_{eq}$, $S_{\alpha\alpha}=S_{\beta\beta}=10^m\times S_{\alpha\beta}$, $m=4$ as follow,

$$\begin{aligned}S_{\alpha\alpha}&=\frac{1}{2}n_{eq}^{-2}\frac{\sigma_{\alpha\beta}}{\gamma} \text{ and}\\ S_{s\alpha}&=\frac{1}{2}n_{eq}^{-2}\frac{\sigma_{\alpha\beta}}{\gamma}\left(1+\frac{1}{2}\cos\theta_0\right) \text{ and}\\ S_{s\beta}&=\frac{1}{2}n_{eq}^{-2}\frac{\sigma_{\alpha\beta}}{\gamma}\left(1-\frac{1}{2}\cos\theta_0\right)\end{aligned} \tag{12}$$

where $\sigma_{\alpha\beta}$ is the surface tension, $S_{\alpha\alpha}$ and $S_{\beta\beta}$ are the strength of the pair force in α and β phases, $S_{\alpha\beta}$ is the strength of the force between α and β fluid phases, $S_{s\alpha}$ and $S_{s\beta}$ are the strength of the pair force between solid and α and β fluid phases, respectively[24]. To implement the neighbor search and time integration for Eqs. (8) and (9), the cell linked list (CLL) and the explicit Velocity-Verlet integration algorithms were used, respectively[19]. Constant time-step size, Δt, and pressure gradient, $\Delta P/L=\rho g$, considered at time integration calculations and creation of steady-state flowing conditions, respectively. The concept of artificial velocity for solid particles proposed by Holmes et al.[13] was used in the modeling of no-slippage boundary conditions on solid walls. Additionally, modification of isotropic pressure parameters and particle number density for solid particles of rock described by Douillet-Grellier et al.[25] is utilized to prevent the unintended entry of fluid particles into the solid walls (or solid grains). Finally, to calculate all properties due to the presence of various boundary types, the correction of the kernel and the gradient introduced by Bonet and Lok[26] was applied.

Method of work

In this study, first, the accuracy of SPH formulation was checked in comparison with proven theoretical methods such as fluid flow within fractures in two kinds of single-phase and two-phase. Then we created the heterogeneous porous medium to investigate the drainage and imbibition processes under partially wetting state ($\theta=(50°, 130°)$) and strongly wetting state ($\theta=(160°, 180°)$). In the next step, the two-phase fluid flow through porous medium under the drainage and imbibition processes was investigated. Finally, the impact of important petroleum reservoir engineering parameters in pore-scale fluid flow such as flow pressure gradient, wettability, and rock heterogeneity was investigated with the help of sensitivity studies on both drainage and imbibition processes (Fig. 1). Also, regular and irregular (randomly) models were generated with known average particle number density within the support radius as proposed by Tartakovsky and Makin[11].

Particle number density and equilibrium pressure for modeling in both regular and irregular models were set at 4 and 144, respectively. For the construction of the randomly generated domains, the initial state is produced by a random distribution of 36 particles within the $9h^2$ as a surface unit and then applying the equilibrium modeling. To perform petrophysical calculations, a series of applied relations introduced in the literature were used[27]. The saturation of each phase is obtained from the ratio of the volume of the phase to the total pore volume of the domain, $S_f=V_f/V_{pv}$. Absolute permeability was calculated using Darcy's relationship as follows,

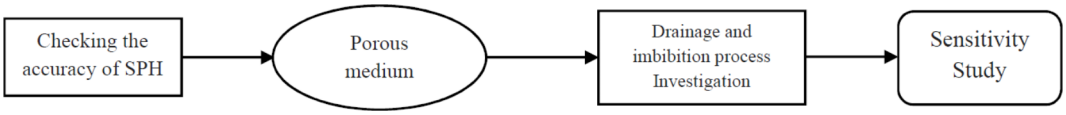

Fig. 1. Flow work of this study.

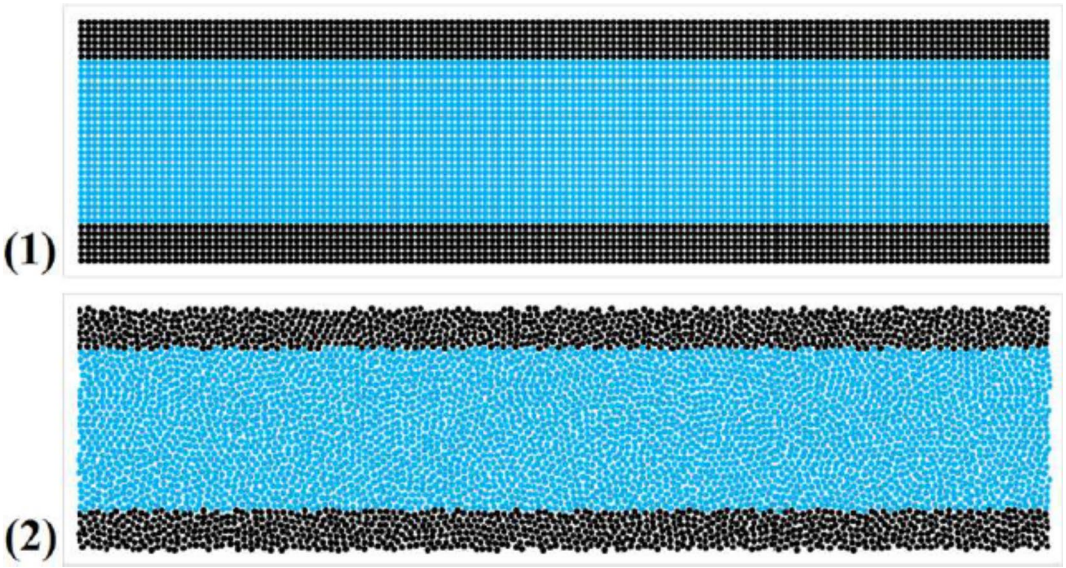

Fig. 2. Schematic of the fracture model used for verification, (1) fracture with smooth surfaces and (2) fracture with rough surfaces (black = solid particles and blue = fluid particles).

$$k = \frac{\mu}{\rho g} \times u_{darcy} \text{ and } u_{darcy} = u_{SPH} \times \emptyset \tag{13}$$

where Ø is porosity. Relative permeability expresses the relationship between absolute permeability (completely saturated with fluid) and effective permeability (in a time when a specific fluid constitutes a fraction of the total pore volume) in a porous medium system. The volumetric flux of the phase and Darcy's relationship were used to determine the effective permeability and relative permeability of each phase α, as shown in the following formula,

$$\vec{Q}_\alpha = \sum \vec{u}_i \times \frac{V_i}{A_i} \text{ and } k_{e\alpha} = \frac{\mu_\alpha}{\rho_\alpha g A \emptyset} \times \vec{Q}_\alpha \text{ and } k_{r\alpha} = \frac{k_{e\alpha}}{k} \tag{14}$$

where k, k_e, and k_r are absolute, effective, and relative permeabilities, respectively. Finally, the recovery factor of each phase can be calculated from $RF=(S_{f\text{-initial}} - S_{f\text{-residual}}) / S_{f\text{-initial}}$.

Verification

Single-phase fluid and two-phase droplet flow within a fracture with soft and rough surfaces were used to verify the formulation of SPH method. To conduct a quantitative investigation, we performed the comparison of the average velocity and permeability between SPH and theoretical results with a calculation of the errors.

Verification of single-phase fluid flow

As shown in Fig. 2, symmetrical and regular particle distribution within the modeling domain results in smooth fracture, whereas random and irregular particle distribution results in rough fracture. 5184 particles in total were scattered evenly with a reduced distance of 0.5 with each other in a square grid to generate the smooth fracture, whereas a random distribution approach introduced before is utilized to generate the fracture with rough surfaces. Additionally, the time-step size of 0.0417 was chosen for the single-phase flow modeling. The domain overall dimensions are 18×72 at x and y, respectively, and the distance between the two surfaces of fracture is 12. As a result, any particle placed outside of the fracture aperture is frozen and converted to solid particles. Therefore, no displacement is taken into account for the particles that are placed out of the fracture aperture and have 3 length units (3 h) from the top and the bottom. Equation 15 presents the Hagen-Poiseuille theory and can be used to calculate the velocity of single-phase fluid flow within the smooth fracture,

		H-P Theory		SPH (Smooth surfaces)			SPH (Rough surfaces)		
g[a]	Time	u[b]	k[c]	u	k	Diff.[d]	u	k	Diff
0.0045	416.667	0.216	12	0.2145	11.92	0.69%	0.2035	11.31	**5.79%**
0.0063	416.667	0.3024	12	0.3038	12.06	0.46%	0.289	11.47	**4.43%**
0.0089	416.667	0.4272	12	0.4302	12.08	0.70%	0.408	11.46	**4.49%**

Table 1. Hagen-Poiseuille theory and SPH results of actual mean velocity and absolute permeability for single-phase flow within fractures. Significant are in value [bold]. [a]Gravitational acceleration. [b]Actual mean velocity. [c]Absolute permeability. [d]Percentage of difference between theory and SPH.

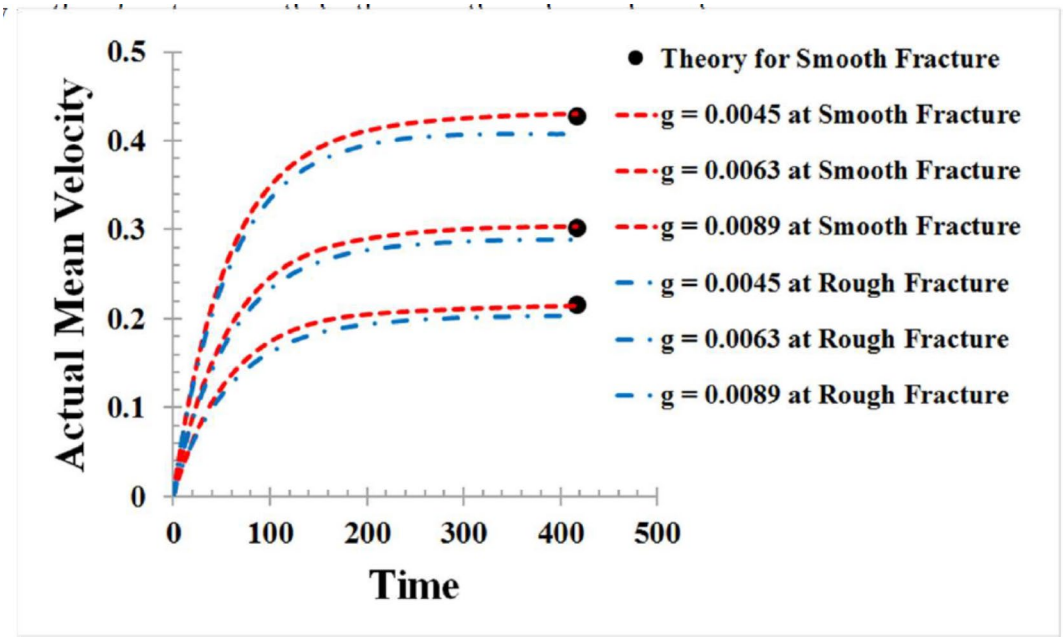

Fig. 3. Actual mean velocity using Hagen-Poiseuille theory (black circles), and SPH for single-phase fluid flow within fractures with smooth (red square dotted lines), and rough (blue rectangular dotted lines) surfaces.

$$u = \frac{b^2}{12\mu}(\rho g) \tag{15}$$

where b is the fracture aperture, μ is the kinematic viscosity, ρ is the mass density, and g is the gravity acceleration. Table 1 lists the calculated (SPH) and theoretical (Hagen-Poiseuille) velocity and absolute permeability for single-phase flow modeling within fracture under three different steady-state pressure gradients in 10,000-time steps. To validate SPH formulation, the theoretical results of the average velocity and absolute permeability were compared to SPH results for single-phase flow modeling through fracture with smooth and rough surfaces. The results in Table 1 show that the history match has been achieved in fracture with smooth surfaces with a difference of less than 1%, and in fracture with rough surfaces with a difference of about 5%. It should be noted that the high difference in the modeling of fracture with rough surfaces is caused by the microscopic roughness of surfaces called friction, S. The results in Table 1 shows that the velocity reduction due to friction in fluid flow through fracture with rough surfaces can be determined by SPH. The absolute permeability for all cases obtained was similar to theoretical results.

The actual mean velocity for both SPH method and Hagen-Poiseuille theory for single-phase fluid flow through fractures (with smooth and rough surfaces) is depicted in Fig. 3. The theoretical value was computed only at stable and final conditions. Although the overall trend is similar for both cases, there is a slight underestimation in actual mean velocity for fractures with rough surfaces caused by friction and surface roughness. Therefore, we experience higher pressure drops (p) and lower actual mean velocity in fractures with rough surfaces compared to smooth ones. This is the reason why red graphs (smooth surfaces) are higher than blue ones (rough surfaces). In general, the possibility of using SPH was also confirmed for single-phase flow within fractures with both smooth and rough surfaces.

Verification of two-phase fluid flow

Figure 4 shows the schematic of placing a fluid drop inside the fracture with rough surfaces and surrounding it with another fluid in equilibrium. Because of the small error between the flowing results of single-phase within fractures with smooth and rough surfaces, the two-phase fluid flow for fracture with a smooth surface was omitted. Fluid drop is chosen with a length of 14.68 and a contact angle of 60° with a solid surface in the wetting condition. In Fig. 4 particles inside the fluid drop are the heavier phase (blue), while the rest of them are in the lighter phase (green). Due to the existence of two immiscible fluids (such as water and hydrocarbon fluids like oil, and gas) in the modeling, a density and viscosity ratio of 1,000 was applied in the verification modeling. Also, an interfacial tension of 5.5 was chosen, and the strength of the pair force of 0.395 between homogeneous particles and 0.0000395 between non-homogeneous particles was determined using Eq. 12 and the parameterization method introduced by Tartakovsky and Panchenko[16]. The wetting conditions of the water fluid with a static contact angle of 60° with solid surfaces were created using the strength of the pair force of 0.4898 between the blue particles with solid surfaces and 0.3002 between the green particles with solid surfaces. To achieve stable modeling by the density and viscosity ratio, a time-step size of 0.00132 was selected for modeling. Equation (16) is the theory of two-phase fluid flow as a drop within fracture with smooth surfaces and can be used to compute the mean velocity of a drop with two advancing and receding contact interfaces. This depicts the first term of the right side of the following equation for single-phase fluid flow as well as the entire right side of the following equation for two-phase fluid flow with two interfaces.

$$u = \frac{b^2}{12\mu}\left(\rho g + \frac{\sigma}{L}\left(\frac{1}{R_a} - \frac{1}{R_r}\right)\right) \tag{16}$$

Also, capillary number for two phase flow considered as follow:

$$N_{ca} = \frac{u\mu}{\sigma} \tag{17}$$

Figure 5 depicts the time evaluation of the droplet flow within the fracture from the equilibrium to the steady state dynamic condition, as well as the final shape of the flowing droplet in the steady state for optional capillary number assuming g to be constant, equal to 0.0114. The shape of the fluid drop and the type of droplet displacement at different time steps can be seen in Fig. 5. As shown in Fig. 5, after reaching time-step 4,000, the drop displacement has reached steady state dynamic conditions, which means that the contact angle hysteresis does not change from that point forward. Figure 5 shows that the advancing contact angle (θ_A) is greater than the receding contact angle (θ_R) at different time steps. This phenomenon is according to the theories in the literature.

The viscosity and mass density ratio of heavy fluid (blue) to light fluid (green) in two-phase fluid flow modeling using SPH is 1,000 times, demonstrating the benefit of using SPH for modeling multi-phase fluid flow through porous medium. The point is that a high ratio reduces the time-step size while increasing the modeling total calculation time. The two-phase fluid flow modeling for verification is done in four different capillary numbers (0.01133, 0.01936, 0.02707, and 0.03909) based on four different pressure gradients (gravitational acceleration). As shown in Fig. 6, increasing g has less effect on increasing the advancing contact angle (θ_A) than decreasing the receding contact angle (θ_R), so a logical contact angle hysteresis is created for both advancing and receding. Table 2 displays the actual mean velocity, effective, and relative permeability for two-phase fluid flow modeling with four gravity accelerations applied in steady-state dynamic conditions. The actual mean velocity, effective, and relative permeability for SPH and the theory were calculated for two-phase fluid flow within fracture with rough surfaces. The results show that the difference in actual mean velocity for four different flow conditions is about 7%. This difference is reasonable for the two-phase fluid flow of the droplet within the fracture with rough surfaces based on the last section and the pressure drop of approximately 5% caused by the existence of microscopic roughness and friction. In addition, effective and relative permeability was obtained near their theoretical values. Figure 7 shows the actual mean velocity time evolution for SPH modeling of the two-phase fluid flow of droplets within fracture with rough surfaces in the presence of theoretical results at the final and equilibrium point. The results of SPH and the theoretical became closer together as the gravity acceleration was reduced.

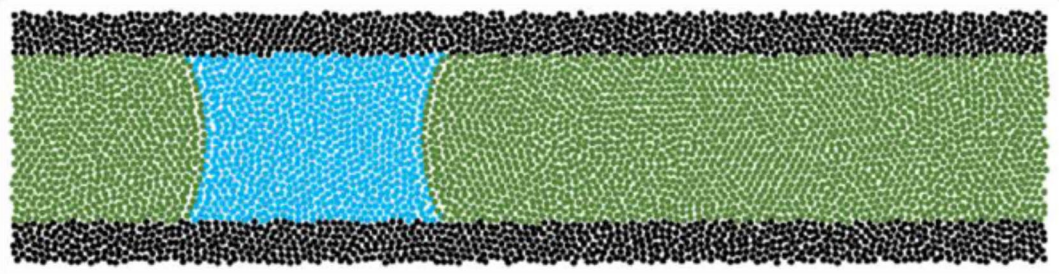

Fig. 4. Schematic of placement of heavy fluid droplet (blue) within the fracture filled with light fluid (green) with contact angle ($\theta = 60^{o}$).

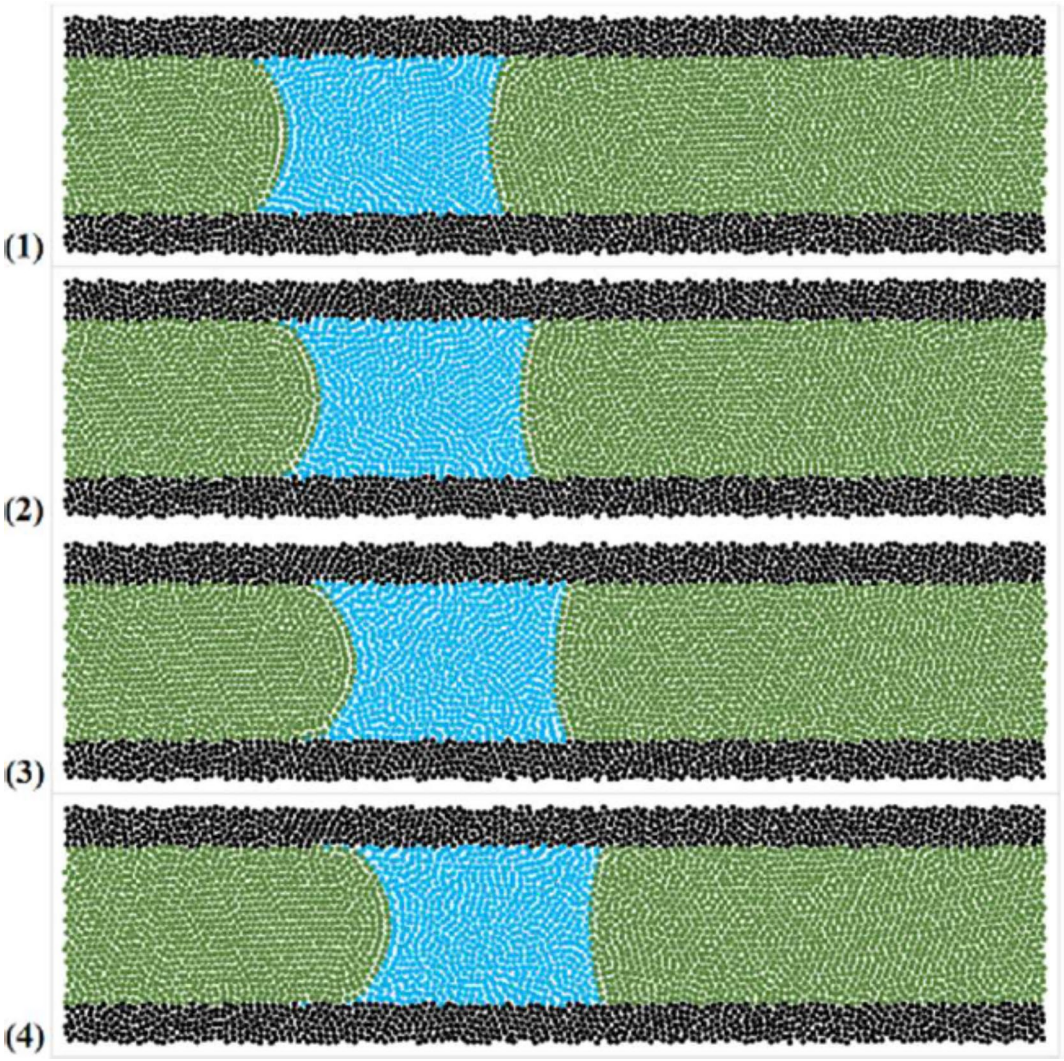

Fig. 5. Time evolution of droplet displacement with g = 0.0114 within the fracture and reaching the steady state in four consecutive time-steps, (1) 10,000, (2) 20,000, (3) 30,000, and (4) 40,000.

Generation of porous medium and modeling domains

The random distribution of solid grains into the modeling domain is employed to generate porous medium with a more realistic configuration to the reservoir rock. The basis of creating a porous medium is based on the method introduced in literature[28]. Three normal distribution functions of solid grain size according to Fig. 8 have been applied for random distribution and creation of the porous medium. The frequency range in the three distributions of solid grains was the same. Finally, solid grains are distributed within three separate domains with the same porosity in a 90 × 30 (reduced) to generate a porous medium. According to these models, the range of solid grain radius for porous medium No. 1, 2, and 3 are 1.18–3.54, 0.92–3.68, and 1.18–3.54, respectively with normal distribution.

After the generation of the three mentioned porous medium, the system dimensions are adjusted to 96 × 30 (reduced) by adding two 3 h-long layers of only fluid particles to prevent the effect of the presence of solid particles on the fluid flow in the direction of applying the pressure gradient. Figure 9 shows the schematic of the generated three irregular porous medium that are used to characterize the drainage and imbibition processes. The total number of particles in all models is 11,519, of which 7466 fluid particles and 4053 solid particles are placed in porous medium No. 1, 7601 fluid particles and 3918 solid particles are placed in porous medium No. 2, and 7730 fluid particles and 3789 solid particles are placed in porous medium No. 3.

Since between the two important parameters of reservoir rock properties (i.e. porosity and permeability), permeability has the greatest impact on the displacement of fluids within porous medium, therefore, various permeabilities were used to have a better investigation in this study. Equation (13) (Darcy's relationship) and single-phase flow modeling through porous medium were used to get absolute permeability. Additionally, each porous medium is divided into two portions in the horizontal direction and the absolute permeability is assessed in each portion to check the permeability distribution. In Table 3, which compares the porosity and permeability of three irregular porous medium, S1 represents the left half (inlet side) and S2 represents the right half (outlet

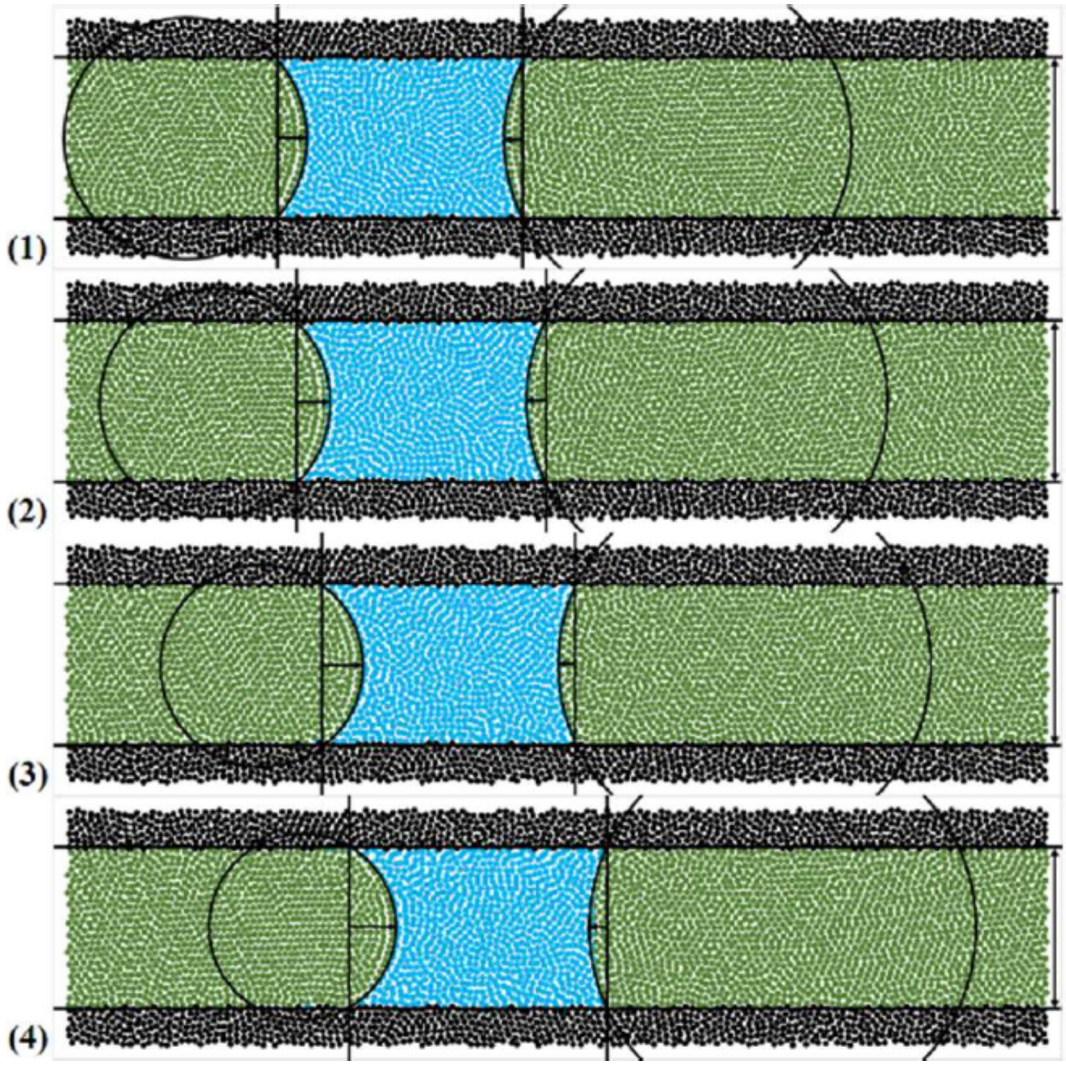

Fig. 6. Final configuration in steady state flow mode for droplet displacement within the fracture with rough surfaces at 4 different capillary numbers, (1) 0.01133, (2) 0.01936, (3) 0.02707, and (4) 0.03909.

		Theory of droplet flow				SPH (Rough surfaces)				
g	Time	u	k	k_e	k_r	u	k	k_e	k_r	Diff
0.0045	65.8808	0.062	12	3.46	0.29	0.065	11.41	3.61	0.32	**4.34%**
0.0063	65.8808	0.106	12	4.23	0.35	0.101	11.41	4.01	0.35	**5.16%**
0.0089	65.8808	0.149	12	4.18	0.35	0.150	11.41	4.21	0.37	**0.75%**
0.0114	65.8808	0.215	12	4.71	0.39	0.200	11.41	4.39	0.38	**6.97%**

Table 2. Theory of droplet flow and SPH results of actual mean velocity, effective and absolute permeability for two-phase fluid flow within fracture with rough surfaces. Significant are in value [bold].

side) of the porous medium. As shown in Table 3 and Fig. 10, the permeability distribution for porous medium No. 1 is homogeneous (uniform distribution of permeability throughout the entire porous medium), whereas for other heterogeneous models (non-uniform distribution of permeability). For porous medium No. 2, the permeability is from a lower value to a higher one, and for porous medium No. 3, the permeability is from a higher value to a lower one. Finally, to model the two-phase flow, the 3 h-long fluid layer attached to the inlet side of the porous medium is changed into the displacing fluid. In this state, there are 359 displacing fluid particles, 7107 displaced fluid particles, and 4053 solid particles in porous medium No. 1. In the porous medium No. 2, there are 359 displacing fluid particles, 7242 displaced fluid particles, and 3918 solid particles There are 359 displacing fluid particles, 7371 displaced fluid particles, and 3789 solid particles in porous medium No. 3.

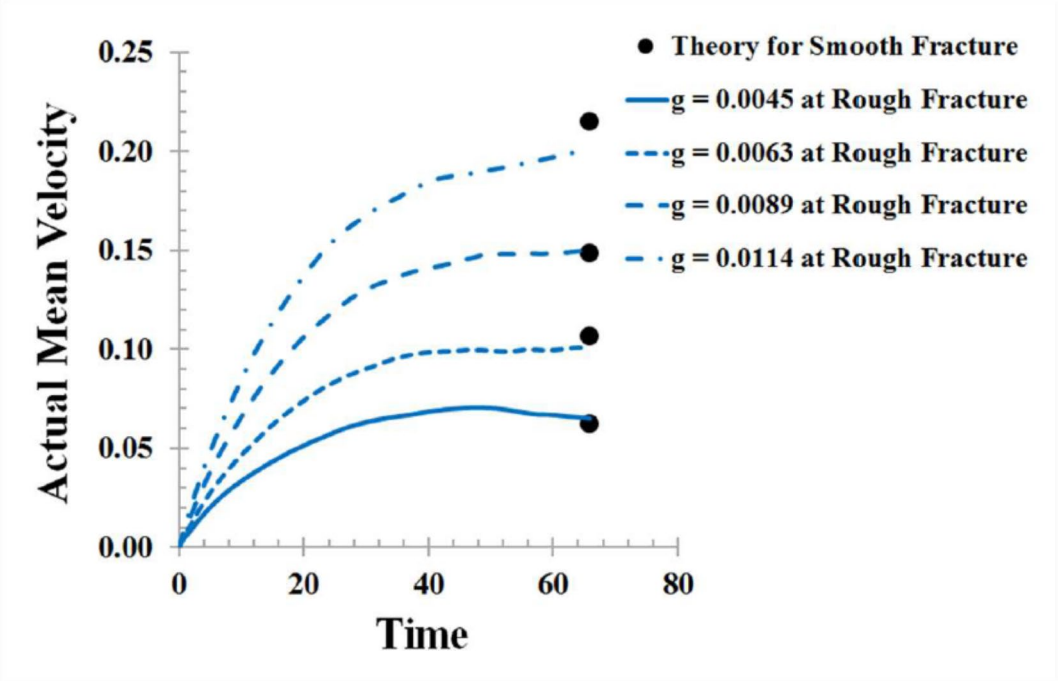

Fig. 7. Actual mean velocity of droplet flow using Eq. 16 (black circles), and SPH for two-phase fluid flow within fracture with rough surfaces (dashed and solid blue lines).

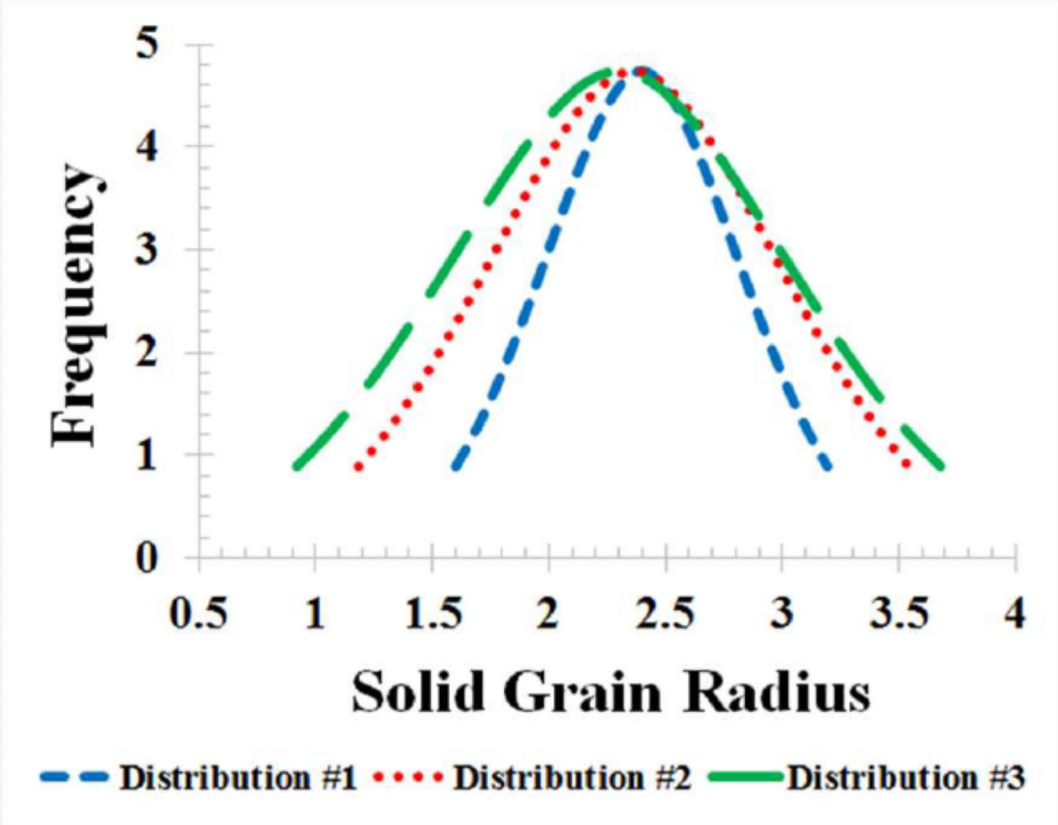

Fig. 8. Normal distribution function for the frequency of solid grain radius used to generate porous medium.

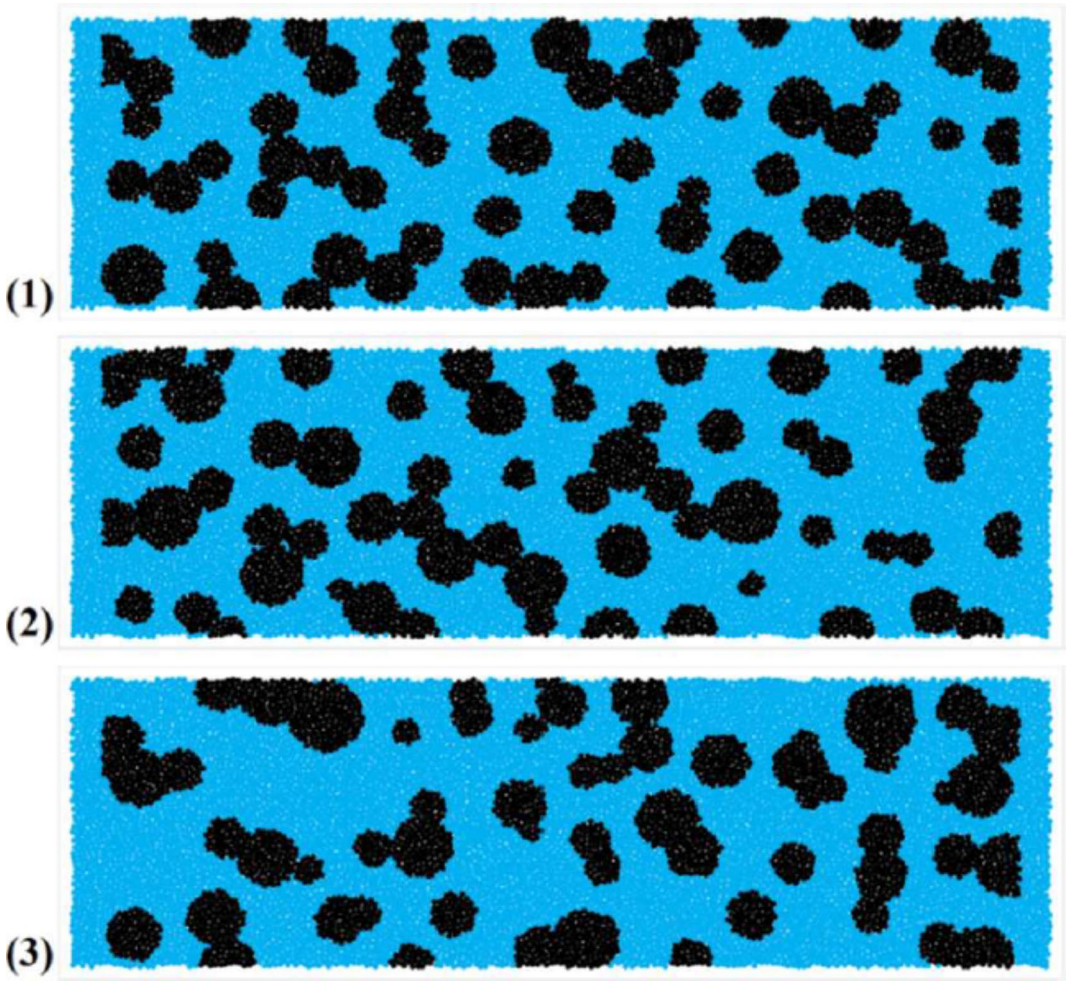

Fig. 9. Schematic of three irregular porous medium generated using normal distribution functions filled with fluid (blue) and solid (black) particles (porous medium No. 1: Ø = 62.47%, porous medium No. 2: Ø = 63.26%, and porous medium No. 3: Ø = 64.04%).

Model	Porosity (Ø)	Permeability (K)
No. 1	62.47%	**0.4431**
No. 1—S1	76.40%	**0.5199**
No. 1—S2	77.41%	**0.5913**
No. 2	63.26%	**0.5228**
No. 2-S1	75.62%	**0.5969**
No. 2-S2	79.47%	**0.7929**
No. 3	64.04%	**0.5855**
No. 3—S1	79.74%	**1.2681**
No. 3—S2	76.48%	**0.5258**

Table 3. Porosity and permeability in different porous medium. Significant are in value [bold].

A mass density and viscosity ratio of 0.5 was also applied for the modeling of two immiscible fluids (such as water with oil, or gas). The mentioned ratio was chosen because high ratios were not employed in two-phase fluid flow modeling to achieve lower time-step size and to decrease modeling run time. The interfacial tension and the strength between similar and non-similar particles were chosen to be the same as the two-phase fluid flow verification model in sections "Verification of two-phase fluid flow". Complete wetting, partially wetting, partially non-wetting, and complete non-wetting were used to model the wetting conditions of the aqueous heavier phase with static contact angles of 0°, 50°, 130°, and 180°, respectively. Equation (12) can be used to calculate the strength of the fluid–solid pair particle interaction forces. By varying the gravity acceleration,

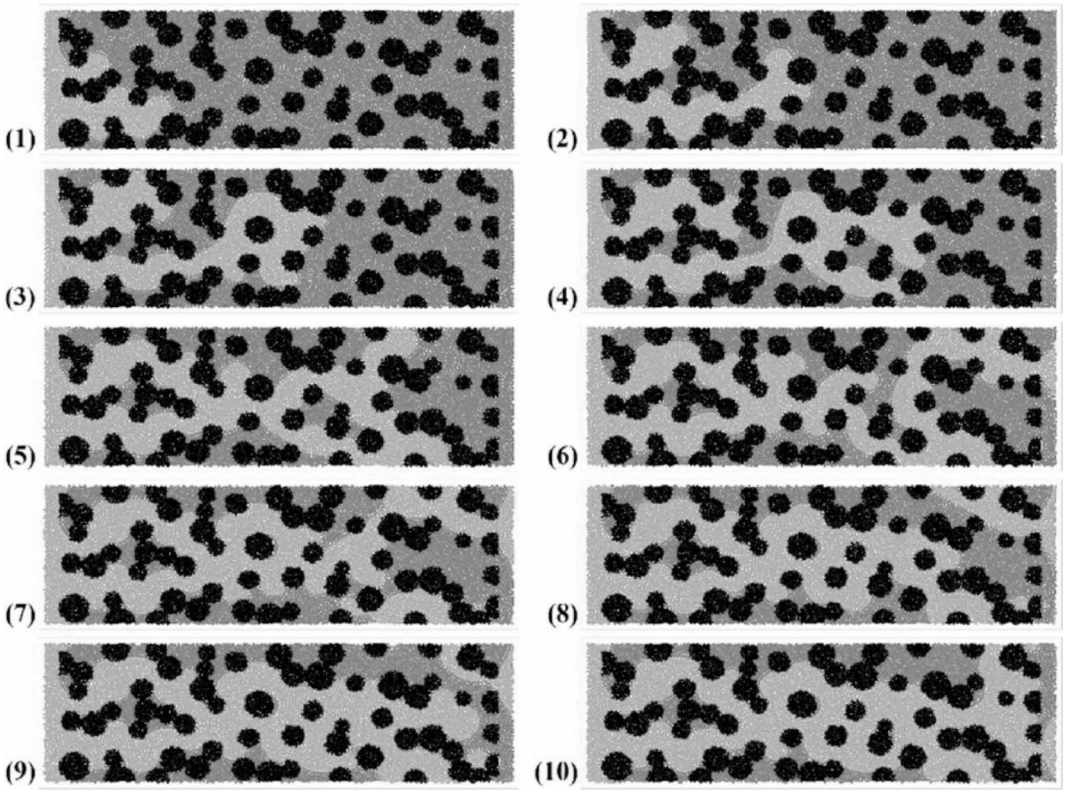

Fig. 10. Color counters of the drainage process in ten consecutive time steps, 5,000 to 50,000 (every 5,000) with $N_{ca} = 0.018$.

varied pressure gradients were produced and used to establish the flow conditions for the entry of the heavier aqueous phase fluid into the porous medium. The time-step size of 0.0295 has been applied to all models.

Results and discussion

Drainage and imbibition process

Drainage is a process where the non-wetting phase is injected into porous medium to displace the wetting phase. It goes against what happens during the imbibition process, in which the wetting phase forces the non-wetting phase out of the porous medium. Since the practical analysis of the drainage and imbibition processes is the main objective of this study, therefore, modeling of the drainage and imbibition processes using SPH with a gravitational acceleration of 0.036 (and $N_{ca} = 0.018$) was done and the results are presented in this section. To model two-phase fluid flow through porous medium, two heavy and light fluids with a viscosity and mass density ratio of 2 were utilized at partially non-wetting and wetting condition for drainage and imbibition processes, respectively. The time hysteresis of the fluid locations as a color counter were examined in every model due to the Lagrangian approach, and particle nature of SPH. Heavy fluids, like water, are depicted in blue, light fluids, like oil, are depicted in green, and rock-solid particles are depicted in black in all color counters.

Figure 10 shows the time evolution of the drainage process over ten consecutive time steps. The hysteresis depicts how the non-wetting fluid displaces the wetting fluid and uses the snap-off mechanism to pass from the larger pores within the porous medium. Since there is less capillary force (or flow resistance) against the non-wetting phase inside the bigger pores during the draining process, the non-wetting fluid attacks the larger ones. It can be seen in Fig. 10 that most displacing non-wetting fluid enters the larger pores. The fingering of the displacing non-wetting fluid through porous medium reveals its high viscosity ratio; therefore, the movement of the displacing non-wetting fluid front is not piston-like. The displacement of secondary displaced wetting fluid fronts and their replacement with displacing non-wetting fluid (Figs. 10–6 and 11) as well as the change in wetting fluid saturation causes the direction of displacement to change after the breakthrough time[29,30].

Figure 11 shows the time evolution of the imbibition process modeling over eight consecutive time steps. As was expected from the definition of the imbibition process, the wetting fluid is displaced by the non-wetting fluid, also, the displacing fluid enters the smaller pores in addition to the larger ones, unlike the drainage process. Therefore, the front of the displacing wetting fluid will be piston-like, as shown in Fig. 11. The breakthrough time occurs faster than the drainage process because the capillary force in the imbibition process is in favor of the wetting fluid flow. The imbibition process does not generate a secondary front or change in the displaced fluid saturation after the breakthrough time in contrast to the drainage process. Additionally, the imbibition process involves much less residual saturation of displaced fluid compared to the drainage process. In the drainage and imbibition processes, the residual saturation of displaced fluid is equal to 28.81% and 8.14%, respectively.

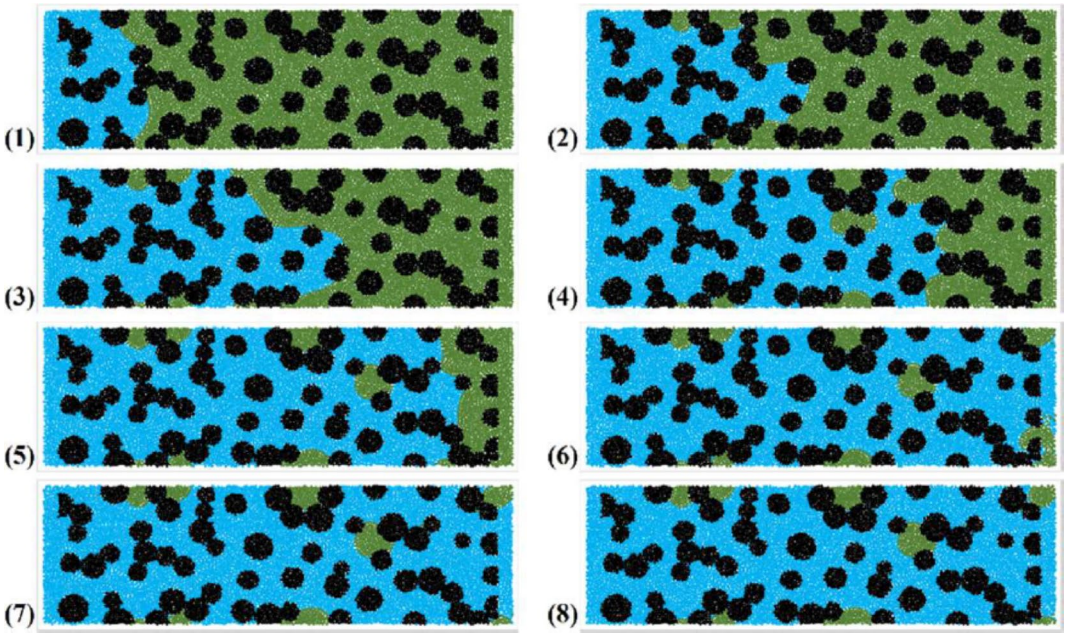

Fig. 11. Color counters of the Imbibition process in eight consecutive time steps, 5,000 to 40,000 (every 5,000) with $N_{ca} = 0.018$.

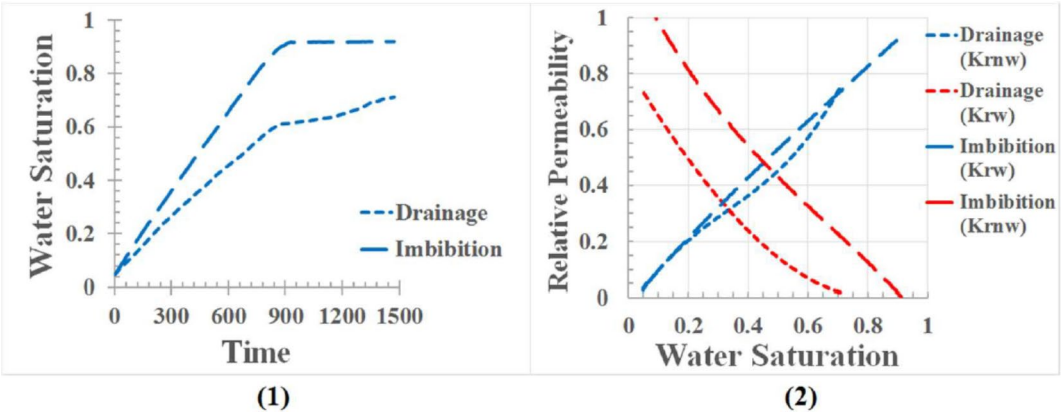

Fig. 12. (1) Time evolution of local saturation and (2) relative permeability curves in the drainage and imbibition processes at partially non-wetting and wetting conditions, respectively.

Additionally, the recovery coefficients in the drainage and imbibition processes are obtained to be 69.73% and 91.45%, respectively[31].

The local changes in fluid saturation and the relative permeability curves are two of the most significant findings about the characterization of the two-phase fluid flow in drainage and imbibition processes which were calculated using Eqs. (13) and (14). using SPH. Figure 12 shows the time evolution of displacing fluid saturation and the relative permeability curves of the two displacing and displaced phases in the drainage and imbibition processes. As shown in Fig. 12-1, the imbibition process reaches a steady state condition more quickly than the drainage process, but the drainage process has not yet reached a steady state condition even after passing a considerable time. The stability time for the steady state condition is when there is no saturation change after reaching that time. After the breakthrough time, the imbibition process is stable, but the drainage process is associated with fluctuations. Fluctuations in the drainage process mean the production of secondary displaced wetting fluid fronts that changes the flowing paths of the non-wetting fluid as observed in the color counters (Fig. 10).

Figure 12-2 depicts the strength of fluid displacement as an important dynamic parameter in the two-phase fluid flow called relative permeability. According to Fig. 12-2, the difference in relative permeability can be seen for the drainage process in the wetting phase and the imbibition process in the non-wetting phase (red graphs), and the velocity of displacement of the phases can also be determined, and compared based on the relative permeability equation. The low velocities of the displacing and displaced fluids can be seen in the

drainage process. It happened because of the existence of the capillary force between the wetting displacing fluid and the non-wetting displaced fluid that the porous medium tends to hold the wetting fluid and resist the entry of the non-wetting fluid. In the Imbibition process, the exact opposite occurs. So, the recovery factor in the imbibition process is higher than the recovery factor in the drainage process. Literature[32] has shown that the relative permeability curve in the two-phase fluid flow through the fracture is in the form of two smooth perpendicular lines, indicating the piston-like displacement of the two-phase interface. Figure 12-2 confirmed the piston-like displacement for the Imbibition process that was previously mentioned (Fig. 11). Additionally, it can be seen in Fig. 12-2 for two-phase fluid flow modeling done in this study that the intersection points in the relative permeability-saturation curve (i.e., $k_{rw}=k_{rnw}$) for the drainage and imbibition processes are always less than 0.5 and about 0.5, respectively. It is clear from the comparisons with the theory of drainage and imbibition processes, that it is possible to perform modeling of these two significant historical processes using SPH and characterize the two-phase fluid flow.

Sensitivity study on pressure gradient

A sensitivity study was performed on different parameters affecting flow dynamics, such as flow pressure gradient, wettability, and heterogeneity. It can demonstrate the application of this study and investigate the maximum feasibility of using SPH in modeling fluid flow through porous medium (i.e., drainage and imbibition processes). Another purpose of the sensitivity studies is to clarify the ideas and theory underlying two-phase fluid flow through a porous medium. The flow pressure gradient (Flow rate) was examined first. Modeling was also repeated for various gravitational acceleration (g) amounts. Figure 13 shows the color counters of the drainage process for the sensitivity study on the flow rate in two different time steps. According to Fig. 13, it can be inferred that as the pressure gradient (i.e., g) increases, so do the flow paths and velocity. The hysteresis of fluid flow through a porous medium is significantly affected by changes in gravitational acceleration, and the residual saturation of the displaced fluid also changes[33,34]. Therefore, the residual saturation of displaced fluid with the recovery factor for gravity acceleration is about 0.018 and 0.072 (or N_{ca} is about 0.009 and 0.036), equal to 62.7% with 34.13% and 25.35% with 73.33%, respectively. In addition, by analyzing the results of the CDC in the experimental tests, the effect of the pressure gradient on the production hysteresis and flowing paths can be seen. This effect of acceleration is also clearly visible in the experimental tests.

In Fig. 14, the imbibition process is shown in two different and consecutive time steps for sensitivity study on the flow rate based on three different gravitational acceleration values, just like the drainage process. Piston-like displacement is seen in all pressure gradients as shown in Fig. 14. However, some dispersed ganglions of displaced fluid still existed within the porous medium. For the imbibition process, a different flow hysteresis is observed for the displacing fluid residue in various gravitational accelerations (g) similar to the drainage process. The velocity of the piston-like displacement of the two-phase interface and the breakthrough time increases with an increase in gravitational acceleration.

Figure 15 shows the time evolution for the local saturation of the displacing fluid in the two processes of drainage and imbibition during the sensitivity study on pressure gradient (flow rate). As the pressure gradient (i.e., g) increases in both processes, the steady state condition is reached more quickly. For the drainage process as shown in Fig. 15-1, stability is not achieved even at low gravitational acceleration (g). As shown in Fig. 15-2, the imbibition process reaches a steady state condition at every gravitational acceleration (g) value. The production of the secondary displaced wetting fluid front is stopped by raising the pressure gradient during the drainage process, which also causes a decrease in the residual saturation. For gravity acceleration values of 0.018 and

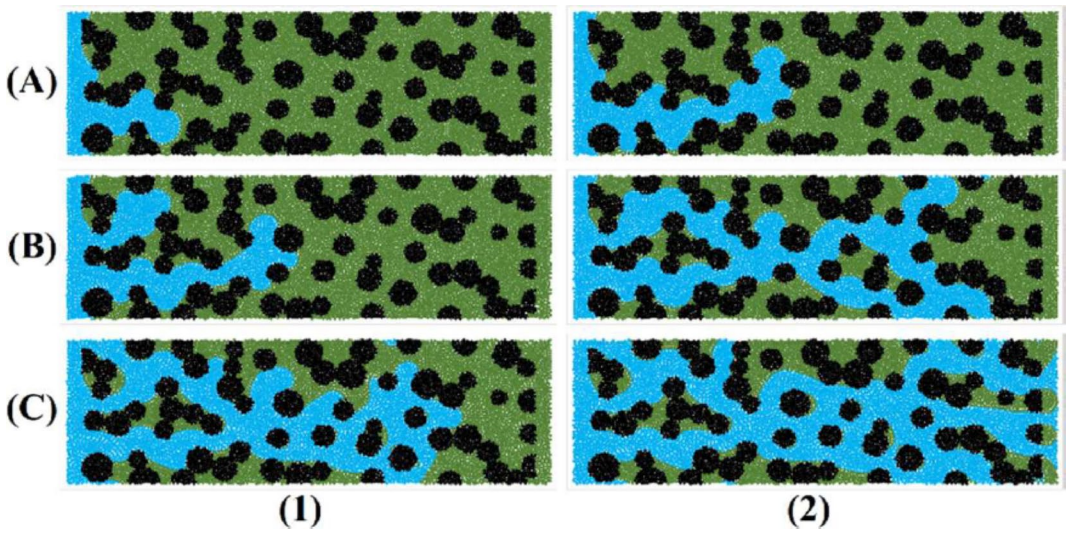

Fig. 13. Color counters of the drainage process for sensitivity study on flow rate at three gravitational accelerations (and N_{ca}), (**A**) 0.018 (and 0.009), (**B**) 0.036 (and 0.018) (basic model), and (**C**) 0.072 (and 0.036), at two time-steps, (1) 10,000 and (2) 25,000.

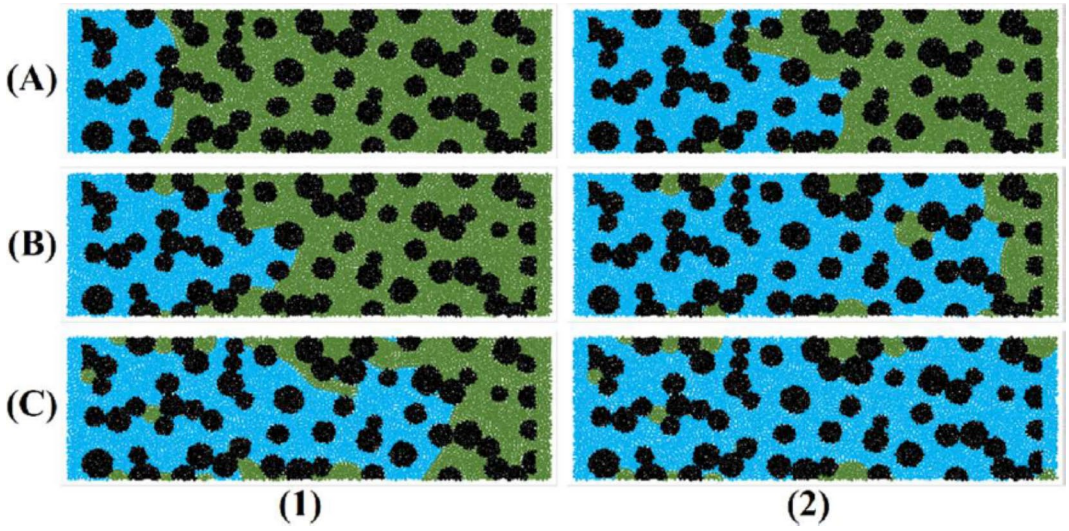

Fig. 14. Color counters of the Imbibition process for sensitivity study on flow rate at three gravitational accelerations (and N_{ca}), (**A**) 0.018 (and 0.009), (**B**) 0.036 (and 0.018) (basic model) and (**C**) 0.072 (and 0.036), at two time-steps, (1) 10,000 and (2) 25,000.

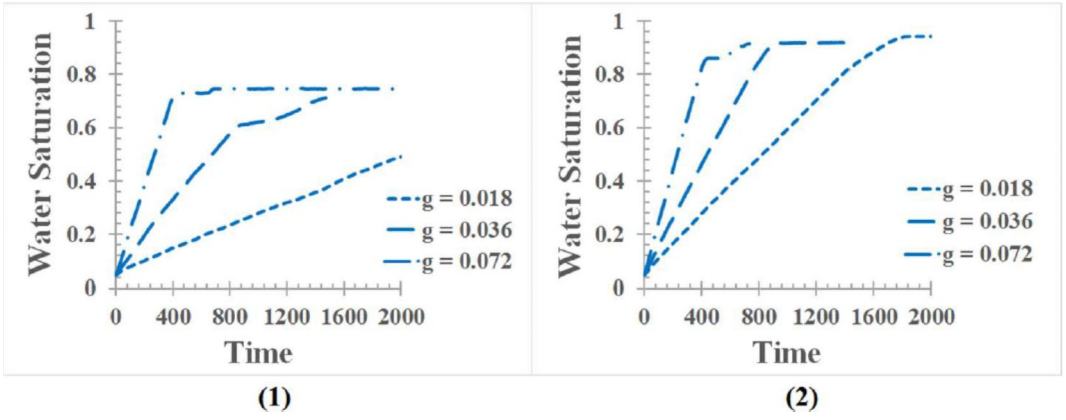

Fig. 15. Time evolution of local saturation in the, (1) drainage, and (2) imbibition processes during sensitivity study on flow rate.

0.072 (or N_{ca} is about 0.009 and 0.036), residual saturation of displaced fluid is about 5.65% and 8.44%, and the recovery factor is 94.06% and 91.13%, respectively. Additionally, it can be concluded that the pressure gradient increases during the imbibition process, increasing residual saturation and formation of secondary displaced non-wetting fluid fronts.

Figure 16 shows the relative permeability curves of two phases in the drainage and imbibition processes during the sensitivity study on the flow pressure gradient. The cross point of two permeability for the drainage process is below 0.5 in different gravitational accelerations. For the imbibition process, due to the piston-like displacement of the front, it is approximately 0.5. When the gravitational acceleration (g) increases for the drainage process, the saturation of the cross-point increases and the displacement process tends to drain wetting fluid more. Consequently, the residual saturation of the displaced fluid decreases, and the recovery factor increases. It is also clear that the flowing paths of wetting and non-wetting fluids with different velocities differ in the drainage process. On the other side, changes in gravitational acceleration (g) during the imbibition process do not have noticeable effects on the relative permeability curve. This is because according to what was mentioned before and the modeling shown in Fig. 14, the displacing wetting fluid front moves like a piston during the imbibition process, and changes in gravitational acceleration only have noticeable effects on breakthrough times. As a result, changes in gravitational acceleration in the imbibition process generally do not show noticeable effects on the relative permeability curve. Even though in the imbibition process, the same residual saturation of the non-wetting fluid with the same recovery factor has been reached at different flowing conditions. The flowing path of the displacing fluid front and its velocity change slightly as gravitational acceleration (g) goes up. The sensitivity study on the flow rate was conducted to see how the drainage and imbibition processes perform within the porous medium[35].

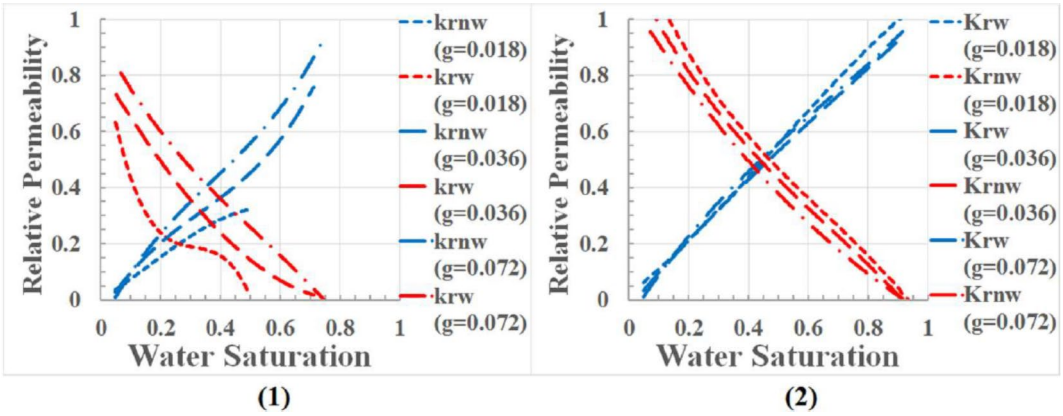

Fig. 16. Relative permeability curves in the, (1) drainage and (2) imbibition processes during the sensitivity study on the flow rate.

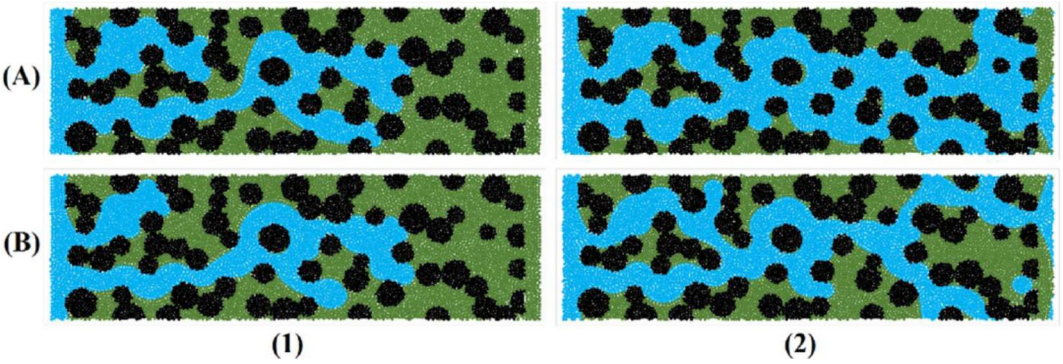

Fig. 17. Color counters in the drainage process for sensitivity study on wettability at two wetting states with $N_{ca} = 0.018$, (**A**) Partially wetting (basic model) and (**B**) Strongly wetting, at two-time steps, (1) 20,000 and (2) 50,000.

Sensitivity study on wettability

For the study of the wettability of the drainage and imbibition processes, the modeling of both processes was repeated with contact angles of 130° and 180° for the drainage and 0° and 50° for the imbibition. Figure 17 shows the color counters during the drainage process in two consecutive time steps for two different wetting conditions. With an increase in the contact angle and a tendency of porous medium for wetting the displaced fluid, the resistance for the entry of the wetting displacing fluid increases significantly. Therefore, the size of flowing paths gets smaller and there is less channeling for displacing non-wetting fluid. As the contact angle increases in the drainage process, it makes it very hard for the displaced non-wetting fluid to get into smaller pores. Also, a different hysteresis of the flow displacement and the residual fluid saturation is seen[36–38]. Because of this, the recovery factor of the displaced wetting fluid goes down as its wetting tendency goes up. Hence the residual saturation and the recovery factor for the drainage process with increasing wettability became 36.62% and 61.53%, respectively.

Figure 18 shows the color counters of flow modeling in two consecutive time steps and two different contact angles for the imbibition process. According to Table 3, which shows the permeability of the generated porous medium used in this study, the porous medium is very tight. Therefore, as a result of increasing the wetting tendency of the displacing fluid, it does not show a noticeable effect on the movement of the displacing wetting fluid front. Therefore, the residual saturation of the displaced fluid and the recovery factor for the imbibition process with increasing wettability are 5.12% and 94.62%, respectively. On the other hand, the breakthrough time and the velocity of the displacing wetting fluid front do not change much in the sensitivity study. The small difference is due to the dispersion and trapping of the displaced non-wetting fluid in both wetting conditions. So, it can be said that the change in contact angle and wettability has more effect on the drainage process than on the imbibition process.

Time evolution in the displacing phase saturation throughout the sensitivity study on wettability for the two processes of drainage and imbibition is depicted in Fig. 19. The discussion presented in Figs. 17 and 18 is more obvious in Fig. 19. As shown in Fig. 19-1, the drainage process under both wetting conditions is still not at its steady state condition. However, the imbibition process always reaches to steady state condition under any wetting conditions as shown in Fig. 19-2. The change in wettability causes a noticeable effect on the drainage

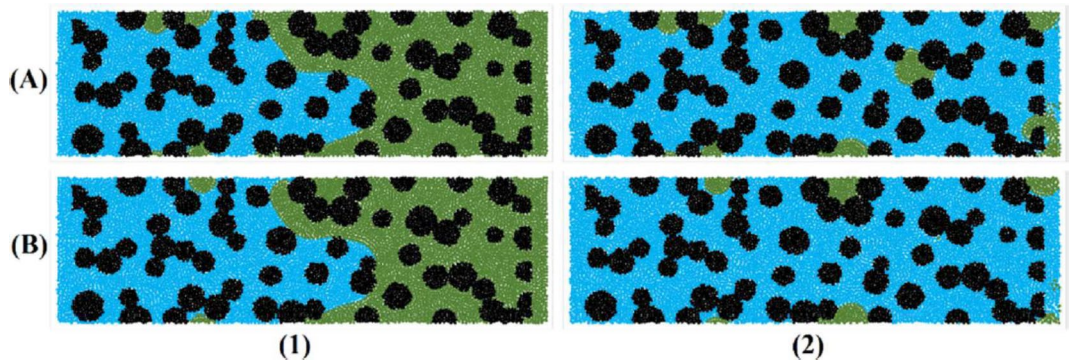

Fig. 18. Color counters in the Imbibition process for sensitivity study on wettability at two wetting states with $N_{ca} = 0.018$, (**A**) Partially wetting (basic model) and (**B**) Non-wetting, at two time-steps, (1) 15,000 and (2) 30,000.

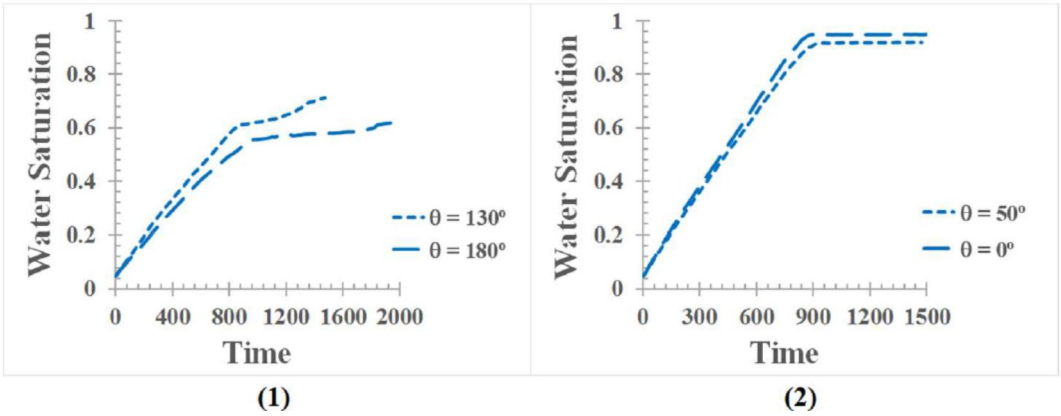

Fig. 19. Time evolution of local saturation in the, (1) drainage and (2) imbibition processes during sensitivity study on wettability.

process and a very small effect on the imbibition process. The production of the secondary displaced fluid front during the drainage process continues with any type of change in wettability, but the frequency of the front generation rises with the increasing tendency of the porous medium to become wetting for displacing fluid (i.e., larger contact angle). After the breakthrough time, the time interval between the formation of each secondary displaced fluid front increases[39].

Figure 20 shows the relative permeability curves in the two processes of drainage and imbibition for the sensitivity study on wettability. The flow behavior (velocity and relative permeability) of the displacing non-wetting fluid is not significantly affected by altering the wettability of the porous medium to the displacing non-wetting fluid during the drainage process. Instead, it decreases the relative permeability of the displaced wetting fluid and moves down the cross point in the relative permeability curve to a lower saturation. The relative permeability curve further shows that the wetting tendency of the porous medium to the displacing fluid had no noticeable impact on the imbibition process. Therefore, the difference in velocity and relative permeability is small and is only a result of dispersion and a small difference in the hysteresis of the fluid flow.

Sensitivity study on morphological heterogeneity

The effect of heterogeneity of the porous medium on the two processes of drainage and imbibition is the last parameter examined in the sensitivity studies. To evaluate the sensitivity of the heterogeneity of the porous medium, two additional porous media were created as explained in section "Verification". For comparison with the basic model (porous medium No. 1) under the same conditions, the modeling of the two processes of drainage and imbibition was repeated in two porous media No. 2 and 3. Figure 21 shows the color counters for the drainage process in the sensitivity study on heterogeneity in three models of porous medium in two consecutive time steps. According to hysteresis, the type of displaced fluid residue and the flowing paths have been impacted by heterogeneity within the porous medium. In porous medium No. 1, where the distribution of permeability is uniform, the dispersion of displaced fluid ganglions within the porous medium is uniform, while the flowing hysteresis of the porous medium No. 2 and 3 have a non-uniform dispersion of ganglions, and also in these two porous medium, most of the residual fluid is in the area of higher permeability. For the two-phase flow, as the drainage process is performed through porous medium No. 2 and 3, the residual saturation

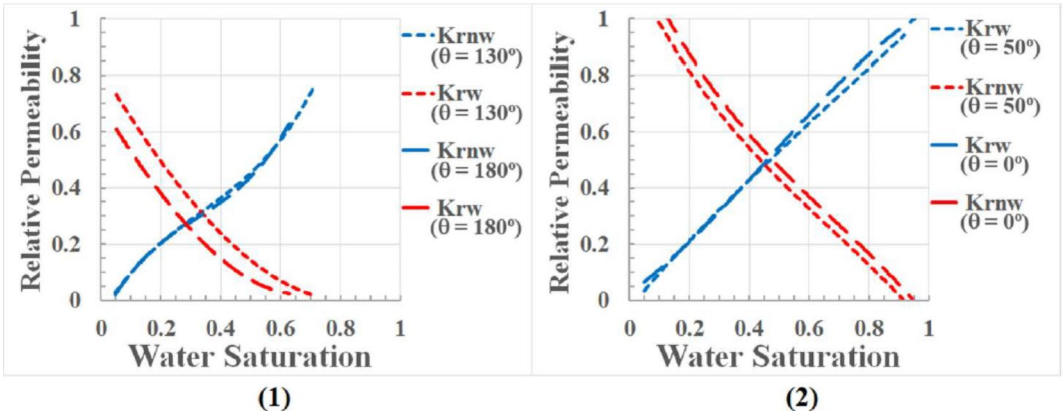

Fig. 20. Relative permeability curves in the, (1) drainage and (2) imbibition processes during sensitivity study on wettability.

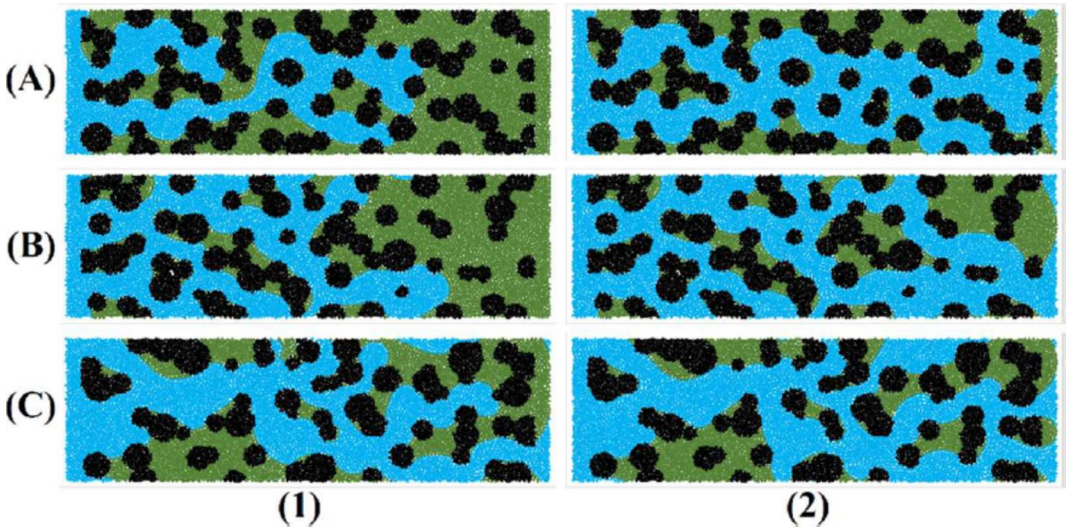

Fig. 21. Color counters in the drainage process for sensitivity study on heterogeneity within three porous medium models with $N_{ca} = 0.018$, (**A**) No. 1 (uniform distribution of permeability) (basic model), (**B**) No. 2 (non-uniform distribution of permeability that is from the lower value to higher one) and (**C**) No.3 (non-uniform permeability distribution that is from a higher value (left side) to lower one (right side)), at two time-steps, (1) 20,000 and (2) 50,000.

of the displaced fluid was 24.30% and 28.16% with the final recovery factor obtained as 74.50% and 70.47%, respectively.

The modeling results of the sensitivity study on heterogeneity for the imbibition process within three existing porous media in two consecutive time steps are shown in Fig. 22. The piston-like displacement of the displacing wetting fluid front is observed in all cases of the porous medium. However, the non-uniform distribution of permeability within the porous medium (No. 2 and 3) makes an obvious difference in the front velocity and the breakthrough time. Also, the different dispersion of displacing fluid ganglions as residual fluid is observed within the porous medium. Also, the volumes of residual displaced fluid in different porous media are small and almost the same due to piston-like displacement. For the two-phase flow of the imbibition process through porous medium No. 2 and 3, the residual saturation of the displaced fluid was 4.04% and 2.98% and the final recovery factor was obtained as 95.76% and 96.88%, respectively.

The time evolution of the displacing phase saturation throughout the sensitivity study on heterogeneity for the two processes of drainage and imbibition is depicted in Fig. 23. The difference in breakthrough time and production or non-production of the secondary displaced fluid front in the drainage process (Fig. 23-1) is observed for various porous media. The departure from the uniformly distributed permeability was shown to lead to quick drainage. It becomes stable faster and stops secondary displaced fluid production. It can also be observed that the imbibition process reaches a steady state condition in all types of porous medium within a given time frame (Fig. 23-2). The residual saturation and the displaced fluid production are seen to be almost

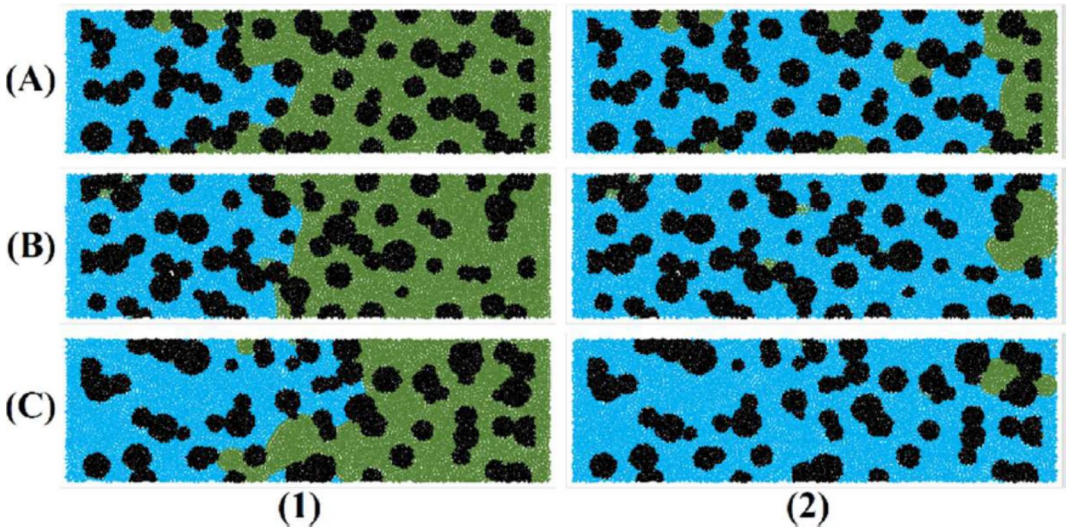

Fig. 22. Color counters in the imbibition process for sensitivity study on heterogeneity for three porous medium models with $N_{ca} = 0.018$, (**A**) No. 1 (uniform distribution of permeability) (basic model), (**B**) No. 2 (non-uniform distribution of permeability that is from the lower value (left side) to higher one (right side)) and (**C**) No. 3 (non-uniform permeability distribution that is from a higher value (left side) to lower one (right side)), at two time-steps, (1) 10,000 and (2) 25,000.

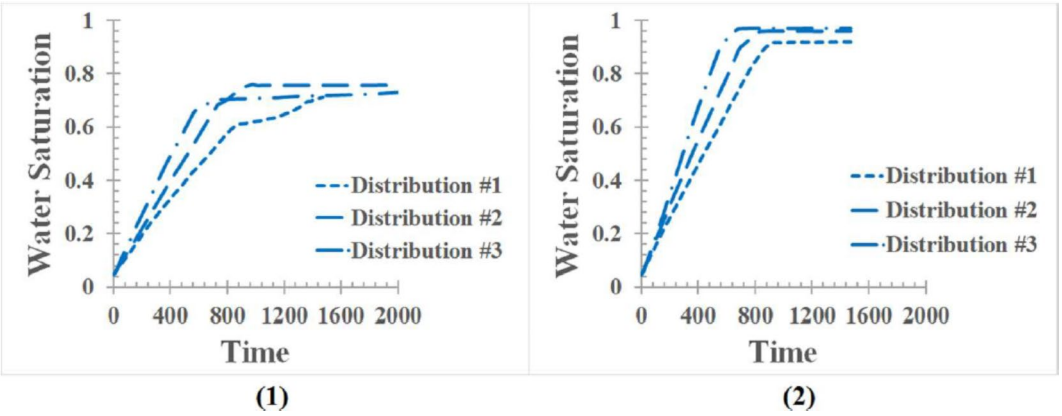

Fig. 23. Time evolution of local saturation in the, (1) drainage and (2) imbibition processes during sensitivity study on heterogeneity.

equal for different heterogeneous models because the recovery factor is more influenced by the porosity than the permeability of the porous medium[40–42].

Figure 24 shows the relative permeability curves of the two processes of drainage and imbibition during the sensitivity study on heterogeneity. The greatest difference between porous medium No. 3 with porous medium No. 1 and 2 is observed in the flow path, velocity, relative permeability, and cross point of relative permeability. However, the influence of porosity on the displaced fluid residual and the recovery factor is more than the influence of the permeability which is confirmed by the relative permeability curves. Therefore, it can be concluded that the heterogeneity in permeability within a porous medium has the greatest impact on the dynamic parameters of fluid flow. Additionally, the cross-point (i.e., $k_{rw} = k_{rnw}$) in the relative permeability curve follows the same pattern as the values below 0.5 and above 0.5 for the drainage and imbibition processes, respectively.

Conclusions

Due to limitations in common simulators, the SPH method was used for fluid flow modeling in a porous medium in this study. This study aims to demonstrate the method's potential in solving petroleum engineering problems. The SPH method has shown promising results in obtaining relative permeability curves and their effect on oil production. The results obtained are as:

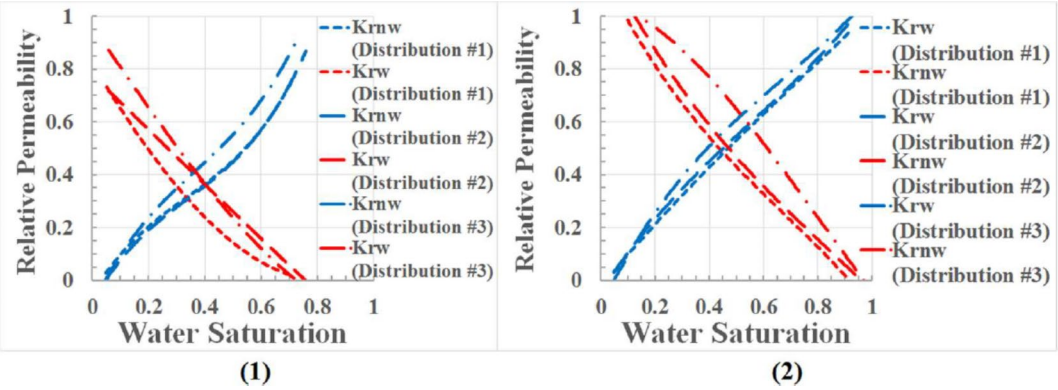

Fig. 24. Relative permeability curves in the, (1) drainage and (2) imbibition processes during sensitivity study on heterogeneity.

1. The verification section of the SPH method formulation is done with the modeling of the single-phase flow in simple and rough fractures and the two-phase droplet movement in the porous medium. The results indicate that history matching was performed in smooth pipes with less than 1% error, and rough pipes with about 5% error. Also, the absolute permeability values were obtained close to the theoretical values. The similarity of the theoretical results to the simulation is more in the smooth surfaces than in the rough surfaces.
2. The results of two-phase verification in the rough surfaces show that the obtained relative permeabilities are very close to the theoretical data. Also, the maximum error obtained in the parameter u SPH is equal to 6.97%, which corresponds to g = 0.0114, and the lowest error is equal to 0.75%, which happened at g = 0.0089.
3. SPH uses an explicit and forward tracking algorithm; therefore, the location profiles such as color counters, local saturation, the velocity of fluids, relative permeability, and recovery factor of the displaced fluids can be easily extracted. The recovery factor can also be calculated using the two dynamic parameters of S_w and K_r. In the majority of drainage processes, there is a multi-stage reaching steady-state conditions with the production of a secondary displacing fluid front. Under certain conditions such as increasing gravitational acceleration and non-uniform distribution of permeability within a porous medium, a quick steady state condition is reached without any production of a secondary displacing fluid front.
4. According to sensitivity studies, pressure gradient (residual saturation of displaced fluid is about 5.65% and 8.44%) and heterogeneity (the residual saturation of the displaced fluid was 4.04% and 2.98%) have the largest impact on flow modeling in both drainage and imbibition processes and wettability (the residual saturation became 36.62% and 5.12%) has only a significant effect on the drainage process within porous medium.
5. In general, fluid flow dynamic studies can be performed using the SPH method to model fluid flow in simple and complex porous media under various flow conditions. The SPH method can also be used as an applicable tool to investigate the hydrocarbon fluids flow within larger geometries in the future.
6. One of the most important achievements of this research is obtaining relative permeability diagrams. These diagrams are one of the main practical data in the study of fluid flow in a porous medium, and their laboratory analysis requires expensive equipment.

Data availability

All data generated or analyzed during this study are included in this published article.

Received: 4 February 2024; Accepted: 17 September 2024
Published online: 27 September 2024

References

1. Su, J., Wang, L., Gu, Z., Zhang, Y. & Chen, C. Advances in pore-scale simulation of oil reservoirs. *Energies (Basel)* **11**(5), 1132 (2018).
2. Lucy, L. B. A numerical approach to the testing of the fission hypothesis. *Astron. J.* **82**, 1013–1024 (1977).
3. Monaghan, J. J. Simulating free surface flows with SPH. *J. Comput. Phys.* **110**(2), 399–406 (1994).
4. Grenier, N., Touze, D. L., Antuono, M., & Colagrossi, A. An improved SPH method for multi-phase simulations. In *Proceedings of the 8nd International Conference on Hydrodynamics*, 2008, vol. 11.
5. Monaghan, J. J. Smoothed particle hydrodynamics. *Annu. Rev. Astron. Astrophys.* **30**, 543–574 (1992).
6. Liu, M. B., Chang, J. Z., Liu, H. T. & Su, T. X. Modeling of contact angles and wetting effects with particle methods. *Int. J. Comput. Methods* **8**(04), 637–651 (2011).
7. Morris, J. P., Fox, P. J. & Zhu, Y. Modeling low Reynolds number incompressible flows using SPH. *J. Comput. Phys.* **136**(1), 214–226 (1997).
8. Zhu, Y. & Fox, P. J. Smoothed particle hydrodynamics model for diffusion through porous medium. *Transp. Porous Medium* **43**(3), 441–471 (2001).
9. Zhu, Y. & Fox, P. J. Simulation of pore-scale dispersion in periodic porous medium using smoothed particle hydrodynamics. *J. Comput. Phys.* **182**(2), 622–645 (2002).
10. Tartakovsky, A. M. & Meakin, P. A smoothed particle hydrodynamics model for miscible flow in three-dimensional fractures and the two-dimensional Rayleigh-Taylor instability. *J. Comput. Phys.* **207**(2), 610–624 (2005).

11. Tartakovsky, A. M. & Meakin, P. Pore scale modeling of immiscible and miscible fluid flows using smoothed particle hydrodynamics. *Adv. Water Resour.* **29**(10), 1464–1478 (2006).
12. Holmes, D., Williams, J., & Tilke, P. Smooth particle hydrodynamics for grain scale multi-phase fluid simulations. In *Proceedings of the 2009 International Conference on Particle-Based Methods* 237–240 (2009).
13. Holmes, D. W., Williams, J. R. & Tilke, P. Smooth particle hydrodynamics simulations of low Reynolds number flows through porous medium. *Int. J. Numer. Anal. Methods Geomech.* **35**(4), 419–437 (2011).
14. Kunz, P. et al. Study of multi-phase flow in porous medium: Comparison of SPH simulations with micro-model experiments. *Transp. Porous Medium* **114**(2), 581–600 (2016).
15. Sigalotti, L. D. G., Rodríguez, C. E. A. & Klapp, J. Application of smoothed particle hydrodynamics (SPH) to flow simulations in oil reservoir rocks. *Int. J. Petrochem. Sci. Eng.* **2**(2), 74–77 (2017).
16. Tartakovsky, A. M. & Panchenko, A. Pairwise force smoothed particle hydrodynamics model for multiphase flow: Surface tension and contact line dynamics. *J. Comput. Phys.* **305**, 1119–1146 (2016).
17. Golparvar, A., Zhou, Y., Wu, K., Ma, J. & Yu, Z. A comprehensive review of pore scale modeling methodologies for multiphase flow in porous medium. *Adv. Geo-Energy Res.* **2**(4), 418–440 (2018).
18. Liu, J., Zhang, T. & Sun, S. Study of the imbibition phenomenon in porous medium by the smoothed particle hydrodynamic (SPH) method. *Entropy* **24**(9), 1212 (2022).
19. Bai, B., Wang, Y., Rao, D. & Bai, F. The effective thermal conductivity of unsaturated porous medium deduced by pore-scale SPH simulation. *Front. Earth Sci. (Lausanne)* **10**, 943853 (2022).
20. Mohammadi, M. & Riazi, M. Applicable investigation of SPH in characterization of fluid flow in uniform and non-uniform periodic porous medium. *Sustainability* **14**(21), 14320 (2022).
21. Liu, G.-R. & Liu, M. B. *Smoothed Particle Hydrodynamics: A Meshfree Particle Method* (World Scientific, 2003).
22. Solenthaler, B., & Pajarola, R. Density Contrast SPH Interfaces (2008).
23. Zhu, Y. I., Fox, P. J. & Morris, J. P. A pore-scale numerical model for flow through porous medium. *Int. J. Numer. Anal. Methods Geomech.* **23**(9), 881–904 (1999).
24. Bandara, U. C. et al. Comparison of pore-scale numerical simulations of unstable immiscible displacements in porous medium with micromodel experiments. *Adv. Water Resour.* **62**, 356–369 (2013).
25. Douillet-Grellier, T., de Vuyst, F., Calandra, H. & Ricoux, P. Simulations of intermittent two-phase flows in pipes using smoothed particle hydrodynamics. *Comput. Fluids* **177**, 101–122 (2018).
26. Bonet, J. & Lok, T.-S. Variational and momentum preservation aspects of smooth particle hydrodynamic formulations. *Comput. Methods Appl. Mech. Eng.* **180**(1–2), 97–115 (1999).
27. Ahmed, T. & McKinney, P. *Advanced Reservoir Engineering* (Elsevier, 2011).
28. Gubaidullin, A. A., Gubkin, A. S., Igoshin, D. E., & Ignatev, P. A. Permeability of model porous medium formed by random discs. In *AIP Conf. Proc.*, vol. 1939, no. March, (2018). https://doi.org/10.1063/1.5027347.
29. Shafiei, M., Kazemzadeh, Y., Shirazy, G. M. & Riazi, M. Evaluating the role of salts on emulsion properties during water-based enhanced oil recovery: Ion type, concentration, and water content. *J. Mol. Liq.* **364**, 120028. https://doi.org/10.1016/j.molliq.2022.120028 (2022).
30. Shafiei, M., Kazemzadeh, Y., Martyushev, D. A., Dai, Z. & Riazi, M. Effect of chemicals on the phase and viscosity behavior of water in oil emulsions. *Sci. Rep.* **13**(1), 1–14. https://doi.org/10.1038/s41598-023-31379-0 (2023).
31. Qin, C. Z. & van Brummelen, H. A dynamic pore-network model for spontaneous imbibition in porous medium. *Adv. Water Resour.* https://doi.org/10.1016/j.advwatres.2019.103420 (2019).
32. Peng, S. Gas-water relative permeability of unconventional reservoir rocks: Hysteresis and influence on production after shut-in. *J. Nat. Gas Sci. Eng.* **82**, 103511. https://doi.org/10.1016/j.jngse.2020.103511 (2020).
33. Ibemesi, P. & Benson, P. Effect of pressure and stress cycles on fluid flow in hydraulically fractured, low-porosity, anisotropic sandstone. *Rock Mech. Rock Eng.* **56**(1), 19–34. https://doi.org/10.1007/s00603-022-03043-y (2023).
34. Arrey, I. A., Odiyo, J. O., Makungo, R. & Kataka, M. O. Effect of hysteresis on water flow in the vadose zone under natural boundary conditions, Siloam Village case study, South Africa. *J. Hydroinform.* **20**(1), 134–148. https://doi.org/10.2166/hydro.2017.091 (2018).
35. Lenormand, R. Numerical models and experiments on immiscible displacement in porous medium, no. November, (2015). https://doi.org/10.1017/S0022112088000953.
36. Zou, S. & Sun, C. X-ray micro-computed imaging of wettability characterization for multiphase flow in porous medium: A review. *Capillarity* **3**(3), 36–44. https://doi.org/10.46690/capi.2020.03.01 (2020).
37. Zhu, Z., Liu, J., Liu, H., Wu, M. & Song, Z. Numerical investigation of single- And two-phase flow in porous medium with a bifurcated fracture. *Phys. Fluids* https://doi.org/10.1063/5.0052229 (2021).
38. Lin, W. et al. Spontaneous imbibition in tight porous medium with different wettability: Pore-scale simulation. *Phys. Fluids* https://doi.org/10.1063/5.0042606 (2021).
39. Yiotis, A., Karadimitriou, N. K., Zarikos, I. & Steeb, H. Pore- scale effects during the transition from capillary - to viscosity - dominated flow dynamics within microfluidic porous - like domains. *Sci. Rep.* https://doi.org/10.1038/s41598-021-83065-8 (2021).
40. Patel, H. S. & Meher, R. Effect of heterogeneity on imbibition phenomena in fluid flow through porous medium with different porous materials. *Nonlinear Eng.* **8**(1), 46–55. https://doi.org/10.1515/nleng-2017-0122 (2019).
41. Mohammadi, M. et al. Application of smoothed particle hydrodynamics for modeling of multiphase fluid flow in non-uniform porous media. *Ind. Eng. Chem. Res.* **62**(33), 13181–13200. https://doi.org/10.1021/acs.iecr.3c01361 (2023).
42. Bagheri, M., Mohammadi, M. & Riazi, M. A review of smoothed particle hydrodynamics. *Comput. Part. Mech.* https://doi.org/10.1007/s40571-023-00679-7 (2023).

Author contributions

Masoud Mohammadi, Masoud Shafiei, Taha Zarin, Yousef Kazemzadeh, Rafat Parsaei and Masoud Riazi, reviewed the manuscript.

Declarations

Competing interests

The authors declare no competing interests..

Additional information

Correspondence and requests for materials should be addressed to Y.K., R.P. or M.R.

Reprints and permissions information is available at www.nature.com/reprints.